Research Division
Rensselaer Polytechnic Institute
Troy, New York

The Use of X-Ray Scattering to Study the Anomalous Elastic Properties of Fe-Ni Alloys

Grant No. DA-31-124-ARO(D)-188*

J. Lawrence Katz
Ronald H. Wilson

31 May 1964

UNPUBLISHED PRELIMINARY DATA

*This work has been supported in part by the National Aeronautics and Space Administration through the Rensselaer Interdisciplinary Materials Research Center.

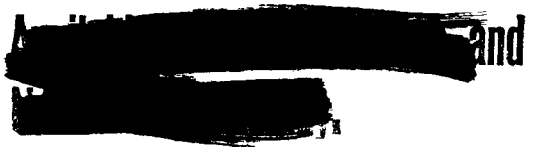

PREFACE

The material contained in this report comprises the dissertation entitled "The Temperature Dependence of the X-Ray Debye Temperature and its Relation to the Elastic Constant Debye Temperature in Nickel and Iron-Nickel Alloys," presented by Ronald H. Wilson in partial fulfillment of the requirements for the degree of "Doctor of Philosophy" at Rensselaer Polytechnic Institute. This degree will be conferred in June 1964.

TABLE OF CONTENTS

LIST OF FIGURES

ABSTRACT

A method for measuring the integrated intensity of Bragg peaks reflected from the face of a large single crystal mounted on a G. E. goniostat at temperatures from 100°K to 600°K is described. In addition, an expression for correcting these intensities for diffuse scattering is presented.

The method has been used on samples of pure nickel and alloys of 29, 31, and 33 percent nickel in iron. X-ray Debye temperatures are calculated from the temperature variation of the Debye-Waller factor. The temperature dependence of these Debye temperatures is compared with the temperature dependence of the Debye temperature calculated from the ultrasonic elastic constant measurements of Alers, Neighbors and Sato (J. Phys. Chem. Solids, 13, 40, 1960).

It is argued that the temperature variation of the two Debye temperatures should agree unless there are contributions to the ultrasonic elastic constants which do not effect the thermal vibrations measured by the x-ray techniques.

Agreement is found for the temperature dependence in the case of nickel in spite of the fact that the size of the Debye temperature from the ultrasonic data is 478°K at room temperature compared with 412°K obtained in this work. Other x-ray methods (Simerska, Czech. J. Phys., 12, 858, 1962) have given about 405°K. This agreement serves as a check on our method.

For the alloys the Debye temperatures calculated from the

ultrasonic measurements of Alers et al. give a change in slope from positive to negative in the Debye temperature versus temperature curve as one goes from below the Curie temperature to above it. Our x-ray measurements do not show this large change in slope. A much smaller change in slope is observed.

It is concluded that the interatomic magnetic exchange energy, J, does not affect the elastic properties of these alloys at the frequencies of the thermal waves important in the x-ray measurements. Such an energy term was introduced by Alers et al. to explain their ultrasonic measurements. This contribution seems necessary to explain the difference between the shear constants in the ultrasonic measurements. Therefore, it is proposed that the effective J value in the ultrasonic measurements is a spatial average of the magnetic exchange energy over the wavelength of the ultrasonic waves; however, for the short wavelengths important in the x-ray measurements this averaging does not smooth out the effects of disorder in the alloys. Thus, the magnetic effect is not seen in the x-ray measurements.

ACKNOWLEDGEMENTS

It is a pleasure to acknowledge the advice and encouragement of my adviser Professor J. L. Katz and of J. S. Kouvel, J. S. Kasper and R. W. Hardt of the General Electric Company. The comments from my graduate committee on the manuscript were appreciated.

In addition I would like to thank Professor Childs and James Frawley of the Metallurgy Department for supplying the nickel sample and assistance in some of the sample preparation.

SECTION I

INTRODUCTION AND HISTORICAL REVIEW

The concept of a temperature related to the maximum frequency of lattice vibrations in a crystaline solid was introduced by Debye (1912) in his work on specific heats. This temperature, known as the Debye temperature, is considered to be characteristic of a solid and is a measure of what can be considered as a high temperature for a given material. In his model Debye assumed the material to be both continuous and isotropic and that the velocity of the thermal vibrational waves is independent of wavelength. The atomic nature of the crystal was introduced by limiting the total number of vibrational modes to three times the number of atoms in the crystal.

Born and von Karman (1912) attacked the problem of determining the vibrational modes in a crystal directly. Subsequent workers have made great progress in calculating the vibrational spectra of crystals (Blackman, 1955; de Launay, 1956). Experimental methods for determining vibrational spectra using x-ray and neutron scattering techniques have been developed and used on a limited number of materials (See a summary in Maradudin, Montrol and Weiss, 1963, Section VII). These methods are difficult and are complicated by uncertainties. However, these experimental and theoretical results do show that the Debye model does not give a good approximation to the true vibrational spectra.

Although it is true that the Debye model is not a good representation of the crystal, the concept of a Debye temperature is

still valid and useful. This is true because the Debye temperature can be introduced into theory through the simple Debye model and later can be evaluated as an experimental parameter which represents an average over the true vibrational spectrum. Such experimental Debye temperatures, their method of measurement, and their theoretical relationship have been reviewed recently by Herbstein (1961).

One of these experimental methods involves the measurement of the intensities of Bragg peaks in the x-ray diffraction. These intensities are attenuated by a factor known as the temperature factor or the Debye-Waller factor. The expression for this factor was first developed by Debye (1914) shortly after his work on specific heats. It was later corrected by Faxen (1918) and then stated in its present form by Waller (1923). These early treatments were classical but later quantum mechanical treatments (Waller, 1928; Ott, 1935; Born, 1942 a,b,c) have verified the correctness of the classical treatments. The classical treatment will be discussed in section III.

The x-ray Debye temperature, Θ_M, which appears in the Debye-Waller factor is introduced through the Debye model. It can be calculated in the Debye approximation with a knowledge of the crystal lattice and the elastic constants of the crystal. The value of Θ_M calculated from the elastic constants will not necessarily agree with the experimental value of Θ_M for several reasons. One reason is that the true vibrational spectrum may differ substantially from the Debye spectrum. Another is that the

elastic constants used in the calculation are usually obtained by methods using frequencies much lower than the frequencies important in the thermal vibrations measured by x-ray techniques.

On the other hand there are methods for calculating the vibrational spectra from the interatomic forces (Blackman, 1955; deLaunay, 1956). These are much closer to the true spectrum than is the Debye spectrum. However, the interatomic forces cannot in general be calculated from first principles so that it is necessary to evaluate them from elastic constant data. When this is done there is still the possibility of errors due to a frequency dependence of the elastic constants. For instance deLaunay (1956) distinguishes between the contribution of the electron gas at ultrasonic frequencies and at thermal frequencies.

Thus, the experimental value of Θ_M can differ from the value calculated from elastic constants for reasons other than differences in vibrational spectra. This fact can obscure the interpretation proposed by Blackman (1956) by which information about the vibrational spectrum could be obtained from a comparison of the calculated and experimental values of Θ_M.

However, there is another aspect of x-ray Debye temperature measurements which can prove useful, i.e. its temperature dependence. There is of course the explicit temperature dependence at very low temperatures in the range $T < \Theta/12$; this temperature dependence has been treated extensively by Blackman (1955). At higher temperatures the explicit temperature dependence is small (Blackman, 1955;

Kagan and Umanskii, 1962; Flinn et al., 1961).

There is a much larger temperature variation of the Debye temperature which is due to the temperature dependence of the interatomic forces. Zener and Bilinsky (1936) and Paskin (1957) have presented theories which relate the temperature dependence of the Debye temperature to the temperature dependence of the lattice constants, i.e. to thermal expansion. The dependence predicted by their theories is generally too low (see the results in Herbstein, 1961). This is not surprising since from the discussion by Huntington (1958) it can be seen that the temperature dependence of the elastic constants cannot be attributed entirely to thermal expansion.

A more direct approach to the temperature dependence of the Debye temperature is to attribute it to the temperature dependence of the elastic constants themselves. From the results in Herbstein (1961) it can be seen that where good experimental values are available the temperature dependence of the Debye temperature can usually be attributed to the temperature dependence of the elastic constants even when the size of the Debye temperatures obtained from the two methods do not agree. This agreement is not surprising if the form of the vibrational spectrum does not vary with temperature since the size of the interatomic forces which determine the vibration spectrum should have the same temperature dependence as the elastic constants. Conversely, deviations from this agreement could be interpreted as failure of one of the above conditions,

i.e. either the form of the vibrational spectrum changes with temperature or the observed elastic constants do not have the same temperature dependence as the elastic properties important in thermal vibrations. The possibility of such an interpretation makes the comparison of the temperature dependence of these calculated and experimental x-ray Debye temperatures a valuable procedure.

A case where such an interpretation can be applied is in the iron-nickel alloy system in the compositions containing about 30 to 45 percent nickel. In these compositions there is a magnetic contribution to the elastic constants which causes a large change in slope of the calculated Θ_M versus T curve as the temperature goes from below the Curie temperature to above the Curie temperature of these ferromagnetic alloys.

In Section II the details of this magnetic effect will be presented. In Section III a development of the Debye-Waller factor will be given to provide the theoretical basis for the interpretation of the x-ray measurements. The experimental procedures for measuring the Debye-Waller factor will be described in Section IV. In Section V the results of our measurements on pure nickel will be compared with previous work as a check on our procedures and then our results for three iron-nickel alloys will be compared with the results of ultrasonic elastic constant calculations. Finally, in Section VI the significance of this comparison will be discussed.

SECTION II

THE MAGNETIC EFFECT IN THE ELASTIC CONSTANTS OF IRON-NICKEL ALLOYS

The anomalous temperature dependence of the elastic constants of face-centered-cubic iron-nickel alloys is well known (Guillaume, 1920; Chevenard, 1920; Engler, 1938; Bozorth, 1950, p. 684). Above the Curie temperatures of these ferromagnetic material the slopes of the elastic constant versus temperature curves are negative with a fractional change of the order of $(10)^{-4}$ per C°. This is about the same as for most metals. Below the Curie temperatures the slopes are very different. Some of this behavior can be attributed to the so-called ΔE effect which derives its name from the observed change in Young's modulus, E, with applied magnetic field. This effect is due to a stress induced change in the direction of magnetization through either domain rotation or domain wall motion. This effect is known to relax out at frequencies of about $(10)^7$ cycles per second (Mason, 1953) and is of no interest in the present work.

There is an additional magnetic effect on the elastic constants which is particularly evident in the composition range of 30 to 45 percent nickel. Alers, Neighbours and Sato (1960, hereafter referred to as ANS) have measured this effect in a single crystal sample by pulse echo ultrasonic methods. Their results are shown in Figure 1 where $C = c_{44}$, $C' = 1/2(c_{11}-c_{12})$ and $B = 1/3(c_{11}+2c_{12})$,

Figure 1

Elastic Constants Versus Temperature
of an Iron—Nickel Alloy with 30% Nickel
Taken from Alers et al.

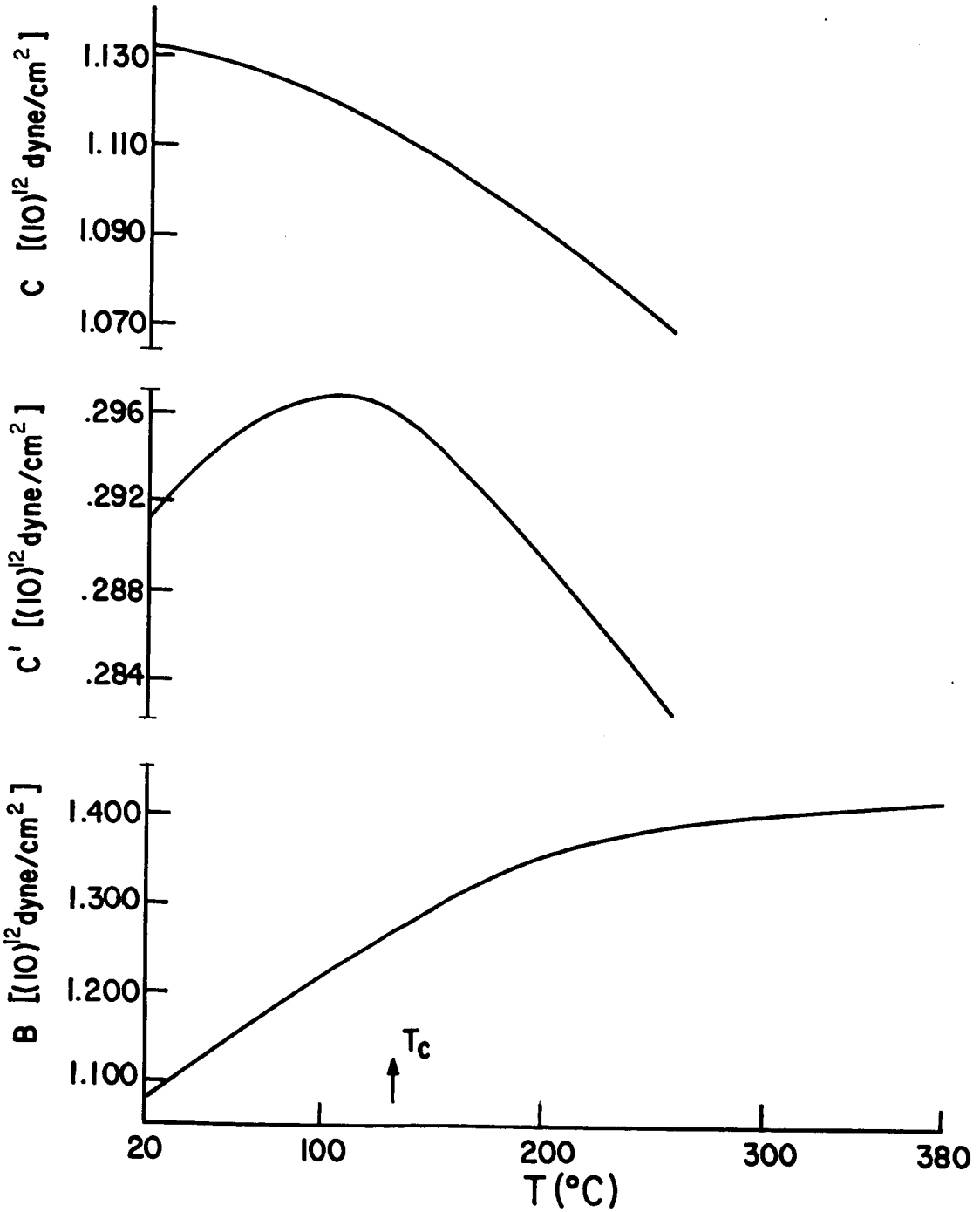
C [(10)^12 dyne/cm^2]
1.130
1.110
1.090
1.070
C' [(10)^12 dyne/cm^2]
.296
.292
.288
.284
B [(10)^12 dyne/cm^2]
1.400
1.300
1.200
1.100
Tc
20
100
200
300
380
T (°C)

i.e. the two shear constants and the bulk modulus respectively. They claim an accuracy of better than one percent absolute, but their results are much more accurate for relative values. It can be seen that the effect is characterized by a marked change in slope near the Curie temperature.

The cause of this effect is generally considered to be a strong dependence of the magnetic exchange energy on interatomic distance. This dependence manifests itself in other ways such as an anomalously low coefficient of expansion (Masumoto, 1931; Owen and Yates, 1937) and an anomalously high volume magnetostriction (for references and discussion see Kouvel and Wilson, 1961). The theory of ferromagnetism in metals is not developed well enough to allow the calculation of this energy from first principles. Therefore, experimental evidence is essential in understanding the nature of this exchange energy.

Apart from any consideration of the cause of these magnetic effects in the elastic constants we can calculate Debye temperatures from the ultrasonic elastic constants measured by ANS. The change in Debye temperature versus temperature for their measurements is shown in Figure 2 as calculated by Anderson's method (O. L. Anderson, 1963: This method is illustrated in appendix F). This behavior will be compared with the observed temperature dependence of the x-ray Debye temperature of similar alloys in Section V.

Figure 2

Debye Temperature Versus Temperature
Calculated from the Elastic Constant Values
of Alers et al.

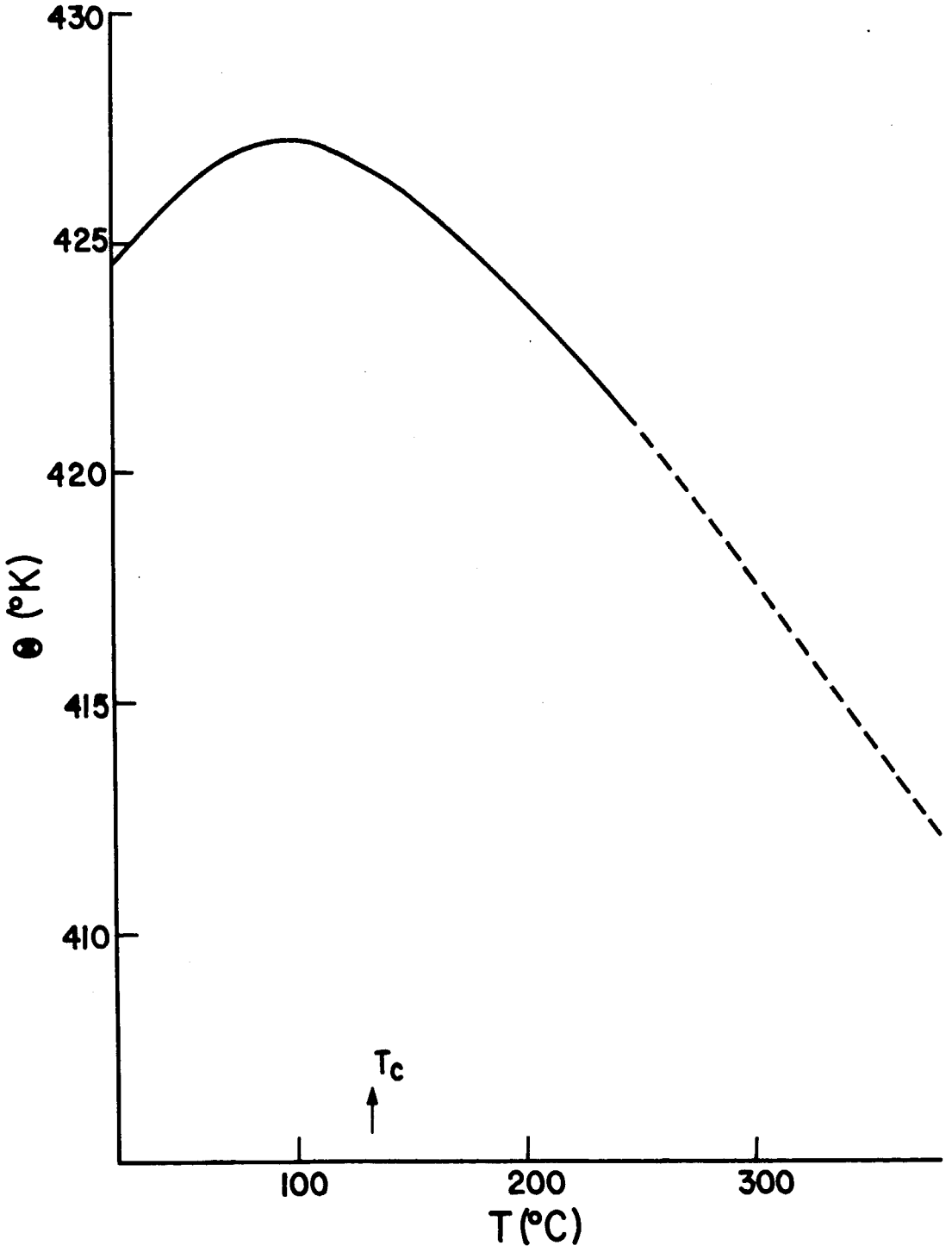
430
425
420
415
410
θ (°K)
Tc
100
200
300
T (°C)

SECTION III

THEORY OF THE DEBYE-WALLER FACTOR

The treatment given here will be similar to that found in James (1954, ch. 5) except our treatment will include structures other than simple cubic. In addition, the assumptions of the Debye model will be introduced in a way to allow easy modification later.

We start with the Fraunhofer diffraction expression for an array of scattering centers at positions $\underline{r}'_n = \underline{r}_n + \underline{u}_n$ with scattering power F which will contain the atomic scattering factor, the polarization factor, the Thompson factor for a radiating electron and the geometric structure factor. The scattered intensity is then:

$$I = F^2 \sum_n \sum_m \exp\left[i \mathcal{K} \underline{S} \cdot (\underline{r}'_n - \underline{r}'_m)\right]$$

$$= F^2 \sum_n \sum_m \exp\left[i \mathcal{K} \underline{S} \cdot (\underline{r}_n - \underline{r}_m)\right] \exp\left[i \mathcal{K} \underline{S} \cdot (\underline{u}_n - \underline{u}_m)\right] \qquad 3.1$$

where $\mathcal{K} = 2\pi/\lambda$ with λ being the wavelength of the radiation; $\underline{S}$ is the scattering vector with magnitude $2 \sin\theta$ where 2θ is scattering angle. When the Laue conditions are satisfied, i.e. at the Bragg peak, then $\theta = \theta_b$ the Bragg angle and $\underline{S} = \underline{S}_0$ a reciprocal lattice vector which is normal to the diffracting plane. We have used $\underline{r}_n$ as the equilibrium lattice position of the nth atom and $\underline{u}_n$ as the displacement of the nth atom from its equilibrium position due to

thermal vibrations. The sum is over all the atoms of the crystal that intercept the incoming beam.

We let

$$p_{n,m} = \kappa \underline{S} \cdot (\underline{u}_n - \underline{u}_m) \qquad 3.2$$

and expand the last factor of equation 3.1 in powers of $p_{n,m}$. Then taking the time average of this factor over a time large compared with the period of thermal vibrations we find that the odd powered terms average to zero because $p_{n,m}$ is as likely to be negative as it is to be positive. Thus, to a good approximation we can write

$$\left\langle e^{i p_{n,m}} \right\rangle = e^{-\frac{1}{2}\langle p_{n,m}^2 \rangle} \qquad 3.3$$

The problem then becomes one of finding the time average of $p_{n,m}^2$.

To do this we consider $\underline{u}_n$ as a superposition of displacements due to all possible thermal waves, so restricting the discussion to acoustic waves, we have

$$\underline{u}_n = \sum_{k\,j} \underline{e}_{kj}\, a_{kj} \cos(\omega_{kj} t - \underline{k} \cdot \underline{r}_n - \delta_{kj}) \qquad 3.4$$

where $\underline{k}$ is a wave vector of magnitude $2\pi/\Lambda$ for a thermal wave of wavelength Λ, $\underline{e}_{kj}$ is a unit vector in the direction of the displacement of the atom due to the kth wave of polarization j (j is one of the three independent directions of vibration), a_{kj} is the

amplitude, ω_{kj} is the angular frequency, and δ_{kj} is the arbitrary phase of the kjth wave.

Using equations 3.2 and 3.4 we have

$$p_{n,m}^2 = \left[\sum_{kj} (\mathcal{A}\underline{S}\cdot\underline{e}_{kj})\, a_{kj}\left\{\cos(\omega_{kj}t - \underline{k}\cdot\underline{r}_n - \delta_{kj}) - \cos(\omega_{kj}t - \underline{k}\cdot\underline{r}_m - \delta_{kj})\right\}\right]^2 \qquad 3.5$$

When the time average is taken all the cross products between different k's and j's average to zero because δ_{kj} is random in time. Then since the time average of $\cos^2\omega t$ is one-half, we have after using a trigonometric identity to modify the last term

$$\frac{1}{2}\langle p_{n,m}^2\rangle = \frac{1}{2}\sum_{kj}(\mathcal{A}\underline{S}\cdot\underline{e}_{kj})^2\langle a_{kj}^2\rangle\left[1 - \cos\left\{\underline{k}\cdot(\underline{r}_n - \underline{r}_m)\right\}\right] \qquad 3.6$$

To obtain an expression for a_{kj} we use similar arguements to get

$$\langle \dot{u}^2\rangle = \frac{1}{2}\sum_{kj}\langle a_{kj}^2\rangle\,\omega_{kj}^2 \qquad 3.7$$

from which the average total vibrational energy (twice the kinetic energy) per atom becomes

$$E = \frac{1}{2}\,m\sum_{kj}\langle a_{kj}^2\rangle\,\omega_{kj}^2 \qquad 3.8$$

where m is the mass of the atom. The total vibrational energy is just the total number of atoms, $\mathcal{N}$, times E. The total energy can

also be written as the sum of the energies in each vibrational wave, E_{kj}, i.e. $\eta E = \sum_{kj} E_{kj}$. Therefore,

$$\langle E_{kj} \rangle = \tfrac{1}{2} m \eta \langle a_{kj}^2 \rangle \omega_{kj}^2 \qquad 3.9$$

But for a harmonic oscillator

$$\langle E_{kj} \rangle = \hbar \omega_{kj} \left[\frac{1}{e^{\hbar \omega_{kj}/kT} - 1} + \frac{1}{2} \right] = \hbar \omega_{kj} \left(n_{kj} + \tfrac{1}{2} \right) \qquad 3.10$$

from which we get

$$\langle a_{kj}^2 \rangle = \frac{2\hbar}{m\eta} \frac{(n_{kj} + \frac{1}{2})}{\omega_{kj}} \qquad 3.11$$

Using this and letting

$$G_{kj} = \frac{\hbar}{m\eta} \frac{(k \underline{S} \cdot \underline{e}_{kj})^2 (n_{kj} + \frac{1}{2})}{\omega_{kj}} \qquad 3.12$$

we have

$$e^{-\frac{1}{2}\langle p_{n,m}^2 \rangle} = e^{-\sum_{kj} G_{kj} \left[1 - \cos\{\underline{k} \cdot (\underline{r}_n - \underline{r}_m)\} \right]}$$

$$= e^{-\sum_{kj} G_{kj}} \; e^{\sum_{kj} G_{kj} \cos\{\underline{k} \cdot (\underline{r}_n - \underline{r}_m)\}} \qquad 3.13$$

so that equation 3.1 becomes

$$I = F^2 \, e^{-\sum_{kj} G_{kj}} \sum_n \sum_m e^{i k \underline{S} \cdot (\underline{r}_n - \underline{r}_m)} \, e^{\sum_{kj} G_{kj} \cos \underline{k} \cdot (\underline{r}_n - \underline{r}_m)} \qquad 3.14$$

Expanding the last exponential in a power series we can write

$$I = I_1 + I_2 + \text{higher order terms} \qquad 3.15$$

where

$$I_1 = F^2 \, e^{-\sum_{kj} G_{kj}} \sum_n \sum_m e^{i k \underline{S} \cdot (\underline{r}_n - \underline{r}_m)} \qquad 3.16$$

and

$$I_2 = F^2 \, e^{-\sum_{kj} G_{kj}} \sum_n \sum_m G_{kj} \, e^{i k \underline{S} \cdot (\underline{r}_n - \underline{r}_m)} \cos\{\underline{k} \cdot (\underline{r}_n - \underline{r}_m)\} \qquad 3.17$$

I_1 is just the Bragg intensity with $e^{-\Sigma_{kj} G_{kj}}$ as the Debye-Waller factor. I_2 is the one phonon diffuse scattering intensity. The other terms give the multi-phonon diffuse scattering intensity. (Maradudin et al., 1963, p. 249). The diffuse scattering will be considered further in appendix A where corrections for its contribution to the measured intensities will be derived. It is the Debye-Waller factor for the Bragg intensity which is of interest here.

The common notation is to write the exponent in the Debye-Waller factor as 2M so that

$$2M = \sum_{kj} G_{kj} \qquad 3.18$$

The first step in the Debye model is to replace the summation over k by an integral. To do this we impose cyclic boundary conditions on the crystal which we assume to be composed of N_1 by N_2 by N_3 unit cells respectively along the three lattice vectors. Cyclic boundary conditions require a phase change of $2\pi p$ (p an integer) over the dimensions of the crystal; for a cubic crystal with lattice parameter, a, we have $k_i N_i a = 2\pi p$ for i = 1, 2, 3. Thus, k takes on discrete values for which we can construct a lattice of spacing $2\pi/N_i a$ with each lattice point representing a possible k value. For a crystal with a large number of cells $N = N_1 N_2 N_3$ and for k not too small the k lattice may be represented by a continum with a density of lattice points given by $N a^3/(2\pi)^3$. Therefore, the number of k values between k and k + dk is given by

$$dN = \frac{N a^3}{(2\pi)^3} 4\pi k^2 dk \qquad 3.19$$

However, since G_{kj} is a function of ω_{kj} we would like to integrate over ω so we introduce the isotropic phase velocity $V = \omega/k$ and the isotropic group velocity $U = \frac{d\omega}{dk}$ for the thermal waves. Then

$$dN = 4\pi N \left(\frac{a}{2\pi}\right)^3 \frac{\omega_j^2}{V_j^2 U_j} d\omega_j \qquad 3.20$$

But the total number of k values per direction of vibration is equal to the number of atoms in the crystal, $\mathcal{N}$. We now define a maximum frequency for the jth polarization, ω_{mj} by

$$\mathcal{N} = \int dN = 4\pi N \left(\frac{a}{2\pi}\right)^3 \int_0^{\omega_{mj}} \frac{\omega_j^2}{V_j^2 U_j}\, d\omega_j \qquad 3.21$$

Again assuming an isotropic medium we replace $(\kappa \underline{S} \cdot \underline{e}_{kj})^2$ by its isotropic average $\kappa^2 S^2/3$ and get

$$2M = \frac{4\pi}{3} \frac{\kappa^2 S^2 \hbar}{m} \frac{N}{\mathcal{N}} \left(\frac{a}{2\pi}\right)^3 \sum_j \int_0^{\omega_{mj}} \frac{(n_{\omega j} + \frac{1}{2})}{V_j^2 U_j}\, \omega_j\, d\omega_j \qquad 3.22$$

Finally, in the Debye model we assume V = U = a constant for all frequencies. Using this assumption in equation 3.21 we get

$$\frac{4\pi}{3} \left(\frac{a}{2\pi}\right)^3 \frac{N}{\mathcal{N}} \frac{1}{V_j^2 U_j} = \frac{1}{\omega_{mj}^3} \qquad 3.23$$

which when substituted into equation 3.22 yields

$$2M = \frac{\kappa^2 S^2 \hbar}{m} \sum_j \frac{1}{\omega_{mj}^3} \int_0^{\omega_{mj}} (n_{\omega j} + \tfrac{1}{2})\, \omega_j\, d\omega_j \qquad 3.24$$

Now, letting $y = \hbar\omega/\kappa T$ and $x_j = \hbar\omega_j/\kappa T$ we get

$$\int_0^{\omega_{mj}} \left(n_{\omega_j} + \tfrac{1}{2}\right) \omega_j \, d\omega_j = \left(\frac{kT}{\hbar}\right)^2 \int_0^{x_j} \left\{ \frac{y}{e^y - 1} + \tfrac{1}{2} y \right\} dy = \omega_{mj}^2 \left\{ \frac{\phi(x_j)}{x_j} + \frac{1}{4} \right\} \qquad 3.25$$

where

$$\phi(x) = \frac{1}{x} \int_0^x \frac{y \, dy}{e^y - 1} \qquad 3.26$$

so that

$$2M = \frac{\kappa^2 S^2 \hbar}{m} \sum_j \frac{1}{\Theta_j} \left\{ \frac{\phi(x_j)}{x_j} + \frac{1}{4} \right\} \qquad 3.27$$

where we have made $\Theta_j = \hbar\omega_j / k$. Equation 3.27 contains three Debye temperatures, one for each vibrational direction. We define a single x-ray Debye temperature, Θ_M, by

$$\frac{3}{\Theta_M} \left\{ \frac{\phi(x_M)}{x_M} + \frac{1}{4} \right\} = \sum_j \frac{1}{\Theta_j} \left\{ \frac{\phi(x_j)}{x_j} + \frac{1}{4} \right\} \qquad 3.28$$

Then noting that $\kappa^2 S^2 = 16 \pi^2 \sin^2\theta / \lambda^2$ we have

$$2M = \frac{12 \hbar^2}{m k} \frac{\sin^2\theta}{\lambda^2} \frac{1}{\Theta_M} \left\{ \frac{\phi(x_M)}{x_M} + \frac{1}{4} \right\} \qquad 3.29$$

which is the usual expression for the exponent in the Debye-Waller factor.

SECTION IV

EXPERIMENTAL PROCEDURES

A. X-Ray Intensity Measurements

To measure the Debye-Waller factor as a function of temperature it is necessary to measure the integrated intensity of Bragg peaks at different temperatures (see Herbstein, 1961, p. 319). There is a broad choice in experimental procedures for making such measurements. We have chosen to measure the integrated intensity reflected from the face of a single crystal larger than the incident x-ray beam. One important aspect of this method is that it is possible to use the same samples both in these measurements and in the ultrasonic measurements. There are difficulties associated with this type of measurement such as surface roughness and the lack of perfect parallelism between the physical surface and the desired crystalographic plane. These difficulties are minimized by the choice of high angle reflections for the measurements. These high angle reflections also tend to maximize the effects to be observed.

Thus, either the (800) or the (660) peak or both were chosen for the measurements. With molybdenum K_α radiation these fall at 2θ angles of about 105° and 115° respectively.

Large grains in ingots prepared from vacuum melted mixtures of high purity iron and nickel in the desired proportions were used. The physical surface was ground and polished in a series of steps until it was parallel to a (100) or a (110) plane of a large grain.

The parallelism was confirmed to within 2° by back reflection Laue photographs. The final step was a chemical or electrical polishing of the surface to remove material cold worked in the grinding process.

The samples were then cemented to 1/8 inch diameter glass rods with Saureisen high temperature cement. The samples were positioned on the rods so that the polished surface could be adjusted to the diffraction plane of a G. E. XRD-5 diffractometer when the rod was inserted in a eucentric goniometer mounted on a G. E. goniostat.

A take-off angle of about 2° was used with a G. E. CA-7 x-ray tube. The beam collimator was that supplied with the G. E. goniostat. The unfiltered beam was directed to the face of the crystal and the reflected x-rays were counted with a scintillation counter with pulse height discrimination. The counter window was 1.2 degrees wide and 2.4 degrees high. This window accepted the full reflected beam.

After alignment, the sample was tested for crystal perfection with an ω motion scan. A symmetrical peak of full width at half intensity of .6 degrees or less was the criterion for acceptance.

A 2θ scan was chosen for the intensity measurements. The scanning rate was .2 degrees per minute. A scan of about 3° was required to include both the K_{α_1}, and the K_{α_2} intensities. Background was counted for 100 seconds at both the starting point and the ending point of the 2θ scan. Thus, the background corrections

include the contributions of the white radiation and the harmonic contributions from other peaks. (Young, 1961) The average of the two background counts was multiplied by the total counting time for the scan and this product was subtracted from the total count accumulated during the scan. This difference was then the measured intensity to which the diffuse scattering corrections (appendicies A and B) were applied to get the integrated intensity. The statistical counting error in this procedure was less than one-half percent but the total error is estimated to be about one percent to allow for uncorrected fluctuations in the source intensity and counting sensitivity.

B. Temperature Control and Measurement

For temperatures above room temperature the crystal was heated by focusing light onto the crystal from a 500 watt DHJ projection lamp with an internal focusing reflector. The temperature was adjusted by varying the voltage to the filament of the lamp. The focal area of the lamp was large enough to include the entire sample but small enough to avoid excessive heating of the goniometer from which the sample was thermally insulated by the glass rod.

For temperatures below room temperature the sample was cooled by a stream of dry nitrogen gas which had been passed through a copper coil immersed in a cryogenic bath. The stream of nitrogen was directed onto the crystal through a special cryostatic

tube with provisions for mixing warm nitrogen with the cold stream to adjust the temperature. It also had an external jacket for directing a defrosting stream around the cold stream.

The temperature of the sample was read by fine wire thermocouples cemented to the sample. The thermocouples were placed so that they would show any significant thermal gradients across the sample. The thermocouples were checked at high temperatures by Tempilaq temperature indicating wax. The linearity of the temperature measurements was established by comparison of the slope of lattice constant versus temperature curves obtained in our measurements with those of similar alloys reported by Owen and Yates (1937).

The estimated error in the temperature determinations at the highest and lowest temperatures is plus or minus 5°.

C. Procedures

Before any intensity measurements were made on it the sample was heated to a temperature higher than any subsequent measurement temperature and held there about one hour. This formed a thin oxide film on the surface of the sample which was not increased in the subsequent measurements.

The intensity data were obtained in a series of runs starting with room temperature measurements; then measurements at other temperatures were made; finally, another measurement at room temperature was made and compared with the first to serve as a check on drift in source intensity or counting sensitivity.

The intensity measurements were made after allowing the sample to equilibrate at some temperature. The next step was to search out the exact position of the peak. The half intensities on both sides of the peak were found for both the χ and ω motions and then these motions were set at positions half way between these. The changes in peak position for motions other than 2θ were only a few hundredths of a degree and could be attributed to slight shifts in the crystal position due to the temperature changes. The changes in 2θ were due to the change in lattice constant with temperature and were used to measure that change. Once the peak was found the 2θ scan was made in exactly the same way for every temperature. The scan range was chosen to be symmetrical with respect to the K_{α_1} and K_{α_2} peaks. Temperatures were read throughout the measurement procedure and excessive drifts in temperature were a basis for throwing out the intensity measurement.

D. Data Reduction

The first step in reducing the intensity data to a useful form was to apply the corrections for diffuse scattering and for lattice expansion as described in appendix B. The intensity can then be written

$$I(T) = I_o \; e^{-2M(T)} \qquad 4.1$$

where I_o is the intensity that would be measured if all of the atoms

were rigidly held at their equilibrium positions. From equation 3.29

$$2M(T) = \frac{12\hbar^2}{mk}\,\frac{\sin^2\theta}{\lambda^2}\,\frac{1}{\Theta_M}\left\{\frac{\phi(x_M)}{x_M} + \frac{1}{4}\right\}$$

$$= A\,\frac{1}{\Theta_M}\left\{\frac{\phi(x_M)}{x_M} + \frac{1}{4}\right\} \qquad 4.2$$

In our measurements I_o is not known so our knowledge is restricted to the intensity relative to the intensity I_R at some reference temperature T_R.

$$I_R = I_o\ e^{-2M_R} \qquad 4.3$$

In our case T_R = 298°K and I_R was our room temperature measurement empirically corrected to 298°K. Thus,

$$\frac{I(T)}{I_R} = \frac{e^{-2M(T)}}{e^{-2M_R}} = e^{-2M(T)+2M_R} \qquad 4.4$$

from which we get

$$\ln\left(\frac{I(T)}{I_R}\right) = -2M(T) - 2M_R$$

or

$$2M(T) = -\ln\left(\frac{I(T)}{I_R}\right) - 2M_R \qquad 4.5$$

If we knew $\Theta_R = \Theta(T_R)$ we could calculate $2M_R$. With $2M_R$ we could calculte 2M(T) for each of the data points. From 2M(T) we can calculate $\Theta(T)$. Unfortunately, Θ_R is not known so it is necessary to assume a value of Θ_R in order to calculate $\Theta(T)$. However, Chipman (1960) has pointed out that the low temperature $\Theta(T)$ values calculated from equation 4.5 are very sensitive to the choice of Θ_R. This restricts the choice of Θ_R to a narrow range if we require physically reasonable Θ versus T curves at low temperatures. Chipman successfully applied such a criterion in his measurements on polycrystaline samples.

The above procedure of assuming a value for Θ_R and calculating a $\Theta(T)$ value for each measured intensity is applied to measurements on our samples in Section V.

SECTION V

RESULTS

Integrated intensity measurements were made over a range of temperatures on four samples: pure nickel and nominal compositions of 29, 31 and 33 atomic percent nickel in iron. A Debye temperature was calculated for each of the intensity measurements by the procedures in Section IV-D. The results of these calculations are shown for our measurements on nickel in Figure 3. Smooth curves drawn through the experimental points are shown for three choices of Θ_R. It can be seen that, except for a narrow range of choices of Θ_R, the low temperature values would show extreme variations which are inconsistent with any physical model. It should be noted that the slope of the high temperature portions of the curves in Figure 3 do not change much from one choice of Θ_R to another.

In Figure 4 is shown the change in Debye temperature for nickel calculated from the elastic constant data of ANS. The result of our x-ray measurements and those of Simerska (1962) are also shown in Figure 4. Error bars are shown indicating the effect of 1% intensity errors and 5°C temperature errors on our data. The value of Θ_R for our data was chosen so that our low temperature data would be consistent with the low temperature elastic constant curve. Simerska's values were obtained from the variation of Bragg intensity with scattering angle; his room temperature value is about 405°K compared with our value of 412°K. This agreement serves as a

Figure 3

Debye Temperature Versus Temperature
from X-ray Measurements on Nickel

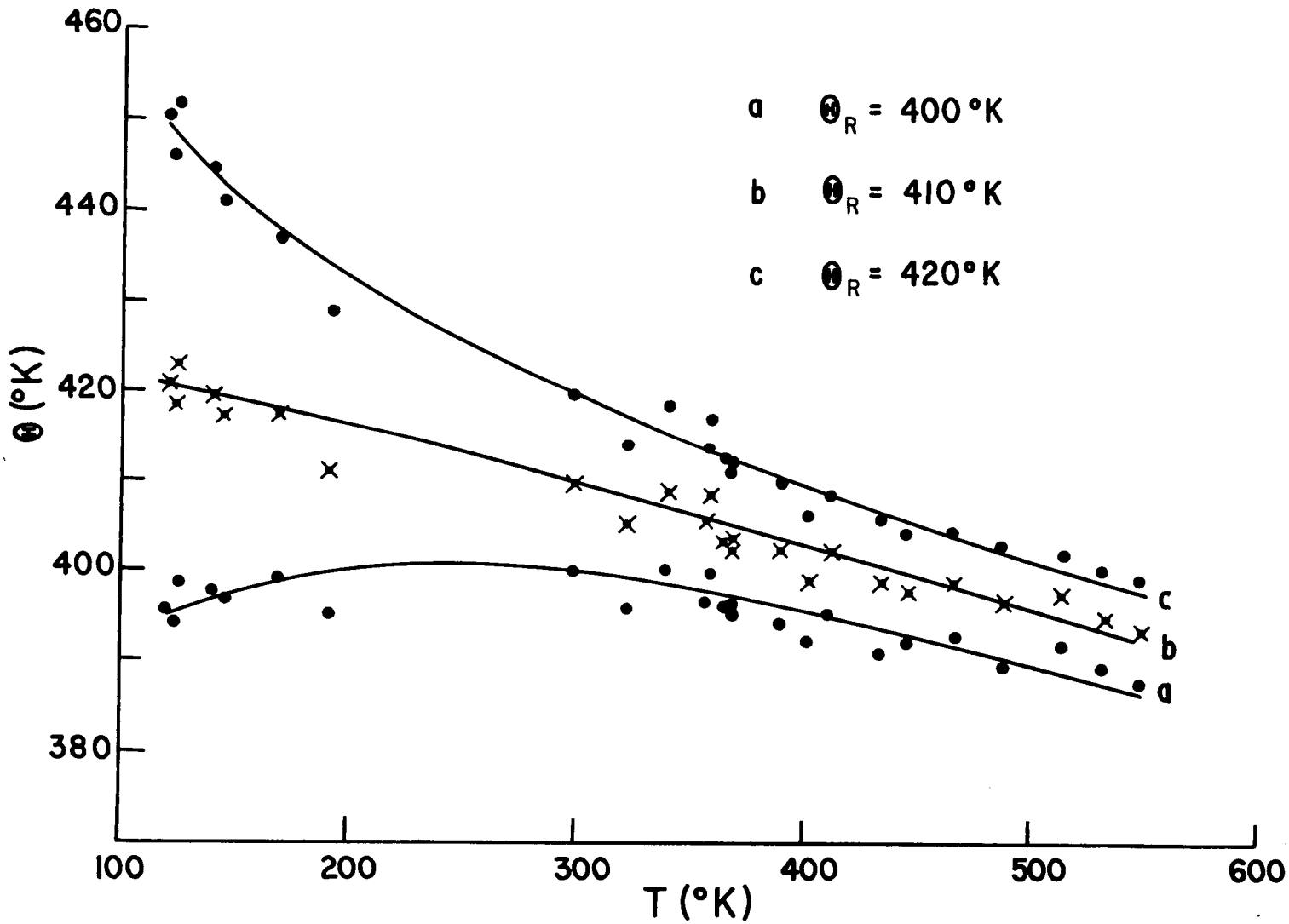
460
440
420
400
380
Θ (°K)
100
200
300
400
500
600
T (°K)
a Θ_R = 400 °K
b Θ_R = 410 °K
c Θ_R = 420 °K
c
b
a

Figure 4

Comparison of the Change in Debye Temperature Versus Temperature from X-ray and Ultrasonic Measurements on Nickel

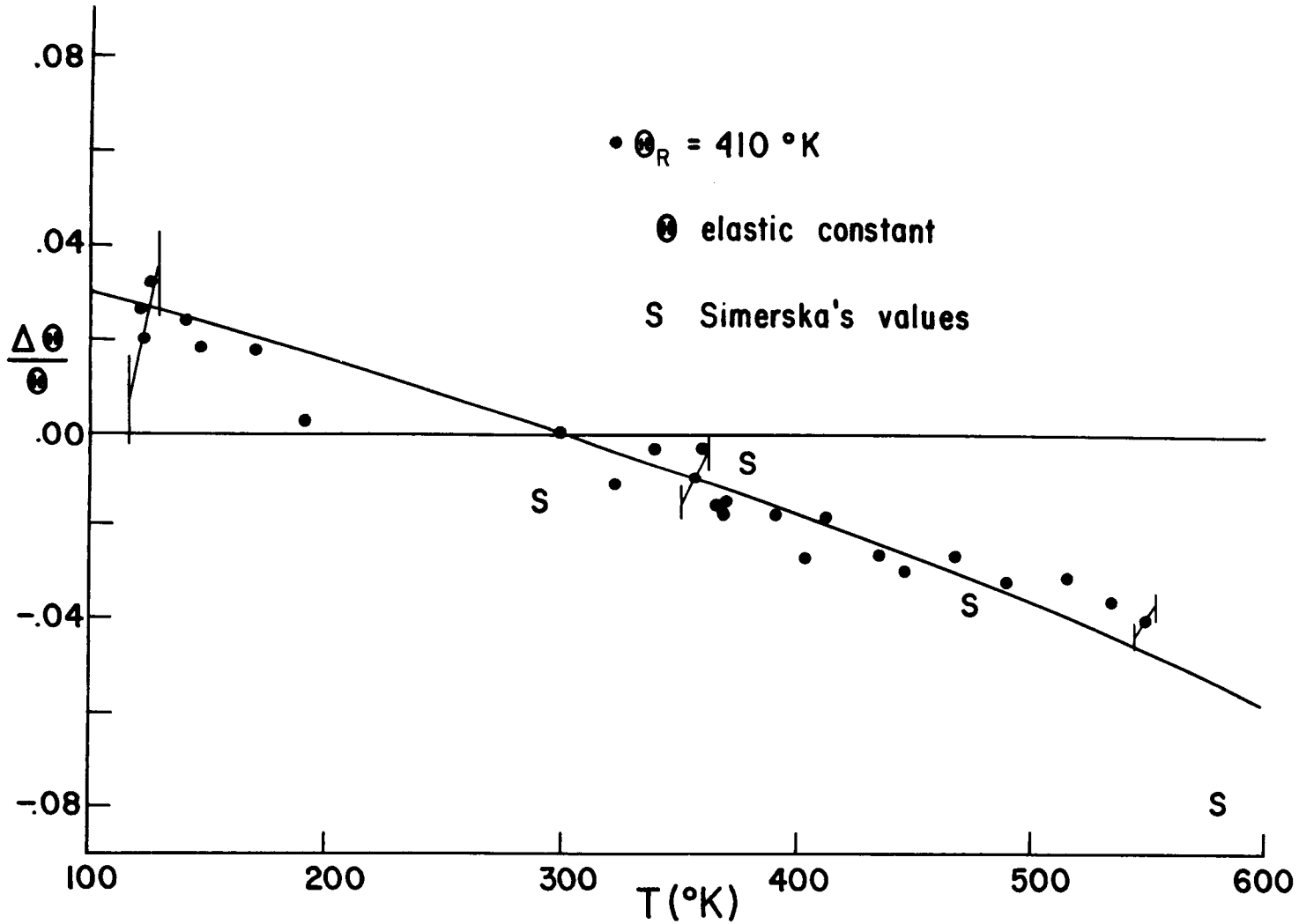
.08
.04
.00
-.04
-.08
$\frac{\Delta\Theta}{\Theta}$
• Θ_R = 410 °K
Θ elastic constant
S Simerska's values
S
S
S
S
100
200
300
400
500
600
T (°K)

check on our procedures. As can be seen in Figure 4, our values fall on the curve from the elastic constant data within experimental error. The room temperature value of Θ calculated from the elastic constant data is 478°K. This illustrates the agreement in temperature dependence between the x-ray and the ultrasonic results despite the disagreement in the size of Θ.

We now turn our attention to the alloys. Since the composition of our alloys was not exactly the same as the alloy measured by ANS, it was necessary to estimate the effect of small composition changes on the elastic constant data in order to make comparisons. The most important factor in the relative position of the elastic constant anomalies is the Curie temperature of the samples. However, in these alloys the Curie temperature is not well defined and may vary with the method of measurement. Fortunately, the lattice parameter, a, versus temperature curves also indicate the temperature of these anomalies. This can be seen in Figure 5 where $\Delta a/a$ versus T is plotted for our alloys along with similar data from ANS. These curves along with Curie temperature measurements made on our alloys were used to estimate the temperature shift of the magnetic anomalies in our alloys relative to the alloy of ANS. The procedure for this and arguments to justify the minor changes in the size of the elastic anomalies in our alloys are given in appendix C.

Measurements were not made on the 29 and 31 percent alloys

Figure 5

Change in Lattice Parameter Versus Temperature
for Our Alloys and The Alloy of Alers et al.

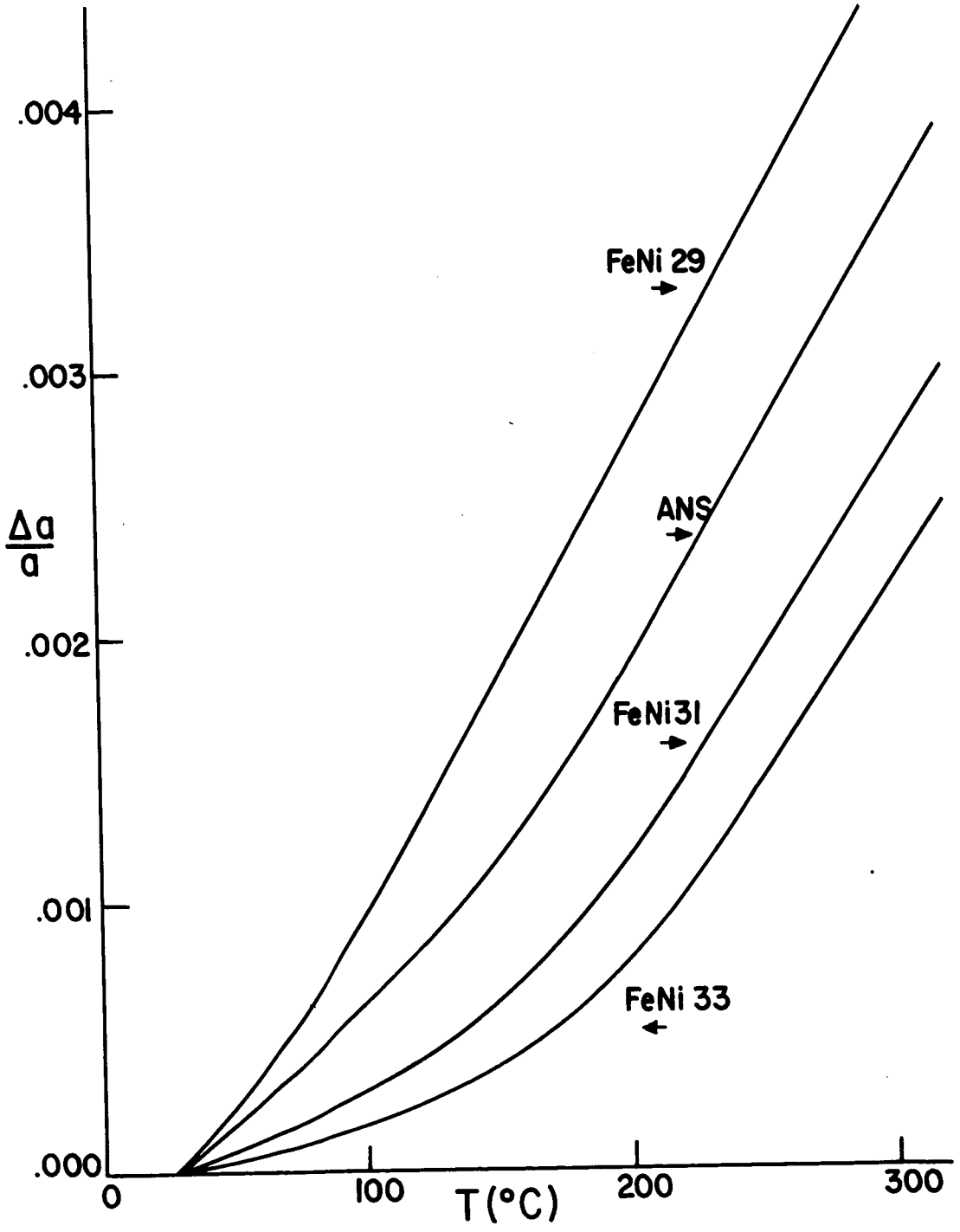
.004
.003
.002
.001
.000
Δa/a
FeNi 29
ANS
FeNi 31
FeNi 33
0
100
200
300
T(°C)

below room temperature because of the low temperature phase transformation that occurs in these alloys. For that reason we will concentrate on the 33 percent alloy first. The solid curve in Figure 6 shows $\Delta\Theta/\Theta$ versus T calculated from the elastic constant data adjusted for the 33 percent alloy. The crossed portion of the curve corresponds to a linear extrapolation of the ANS data into the low temperature region. Based on the nature of the magnetic effects it is expected that any deviation from this linearity should be an upward curvature at the lowest temperatures. The dashed curves show $\Delta\Theta/\Theta$ versus T as determined from our experimental points for several choices of Θ_R. The individual data points from which these curves were determined are shown for only one curve to avoid confusion. The curves are drawn to coincide at a temperature above the Curie temperature because the magnetic effects should be small there. As the temperature is lowered past the Curie temperature the magnetic effects become large and show up as a large change in slope in the elastic constant curve. It can be seen that a comparable change in slope does not occur in the x-ray data. It can also be seen from Figure 6 that this conclusion is not sensitive to the choice of Θ_R. Even the obviously low choice of Θ_R for curve a does not produce a change in slope comparable to that in the elastic constant results.

On the other hand, the x-ray curves show a smaller but definite change in slope near the Curie temperature. Thus, there

Figure 6

Change in Debye Temperature Versus
Temperature for the 33 Percent Nickel Alloy

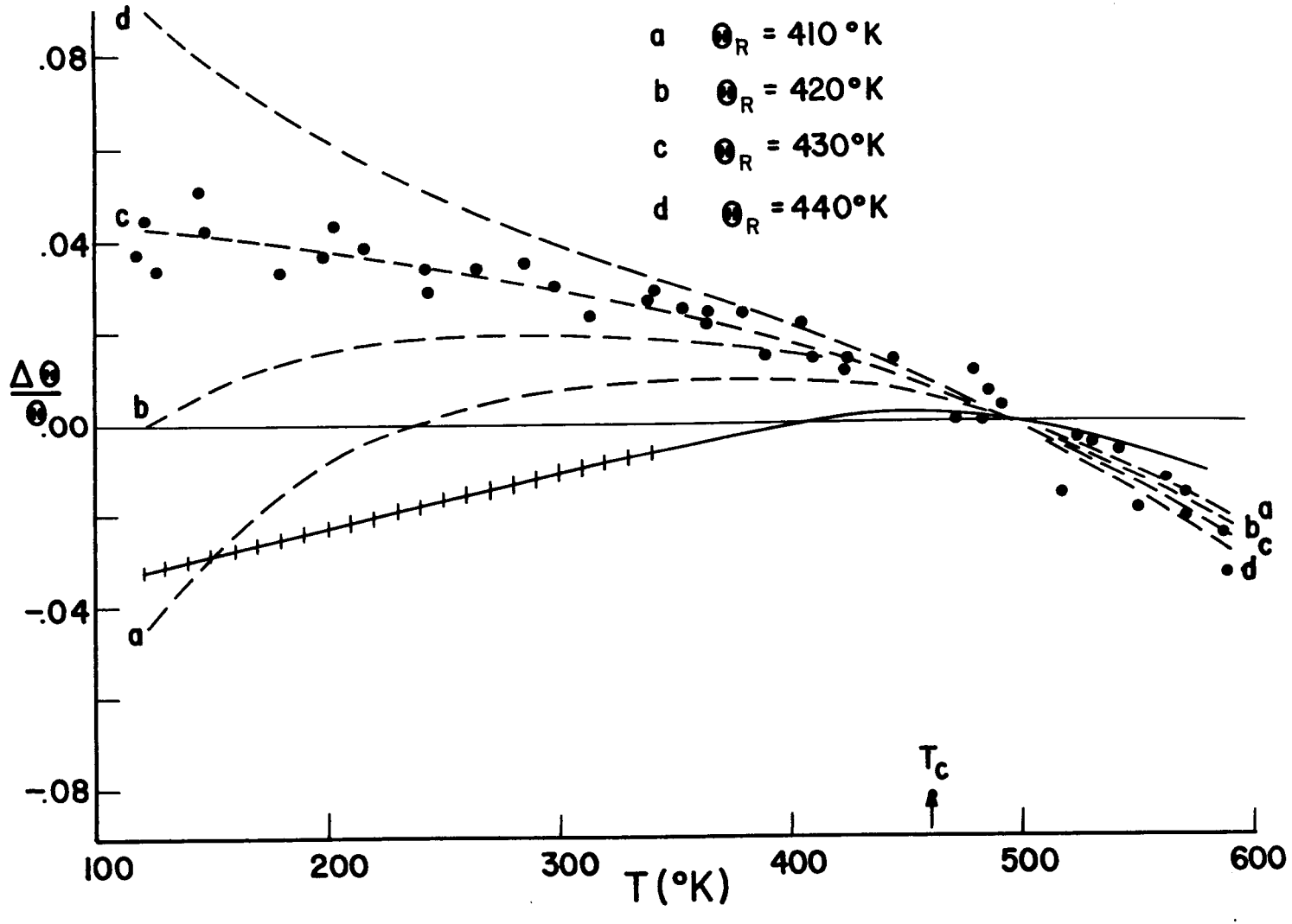
a Θ_R = 410°K
b Θ_R = 420°K
c Θ_R = 430°K
d Θ_R = 440°K
.08
.04
.00
-.04
-.08
$\frac{\Delta\Theta}{\Theta}$
100
200
300
400
500
600
T(°K)
T_c

must be some manifestation of the magnetic effects in the x-ray data. Possible explanations of these results will be discussed in the next section.

The data for the 29 and 31 percent samples are shown in Figure 7. These results are less definitive for two reasons. First, the Curie temperatures are lower and therefore, the critical region below the Curie temperature is in a temperature range which is more sensitive to the choice of Θ_K. Second, the lack of low temperature data makes the choice of Θ_K less certain. However, the data for the 31 percent sample seem to support the conclusions drawn from the 33 percent sample. The data for the 29 percent sample are at least not inconsistent with those conclusions.

The differences in slope above the Curie temperature are attributed to the persistence of some magnetic effects even above the Curie temperature. This is readily seen in the curve for B shown in Figure 1.

Figure 7

Change in Debye Temperature Versus Temperature

for the 29 and 31 Percent Nickel Alloys

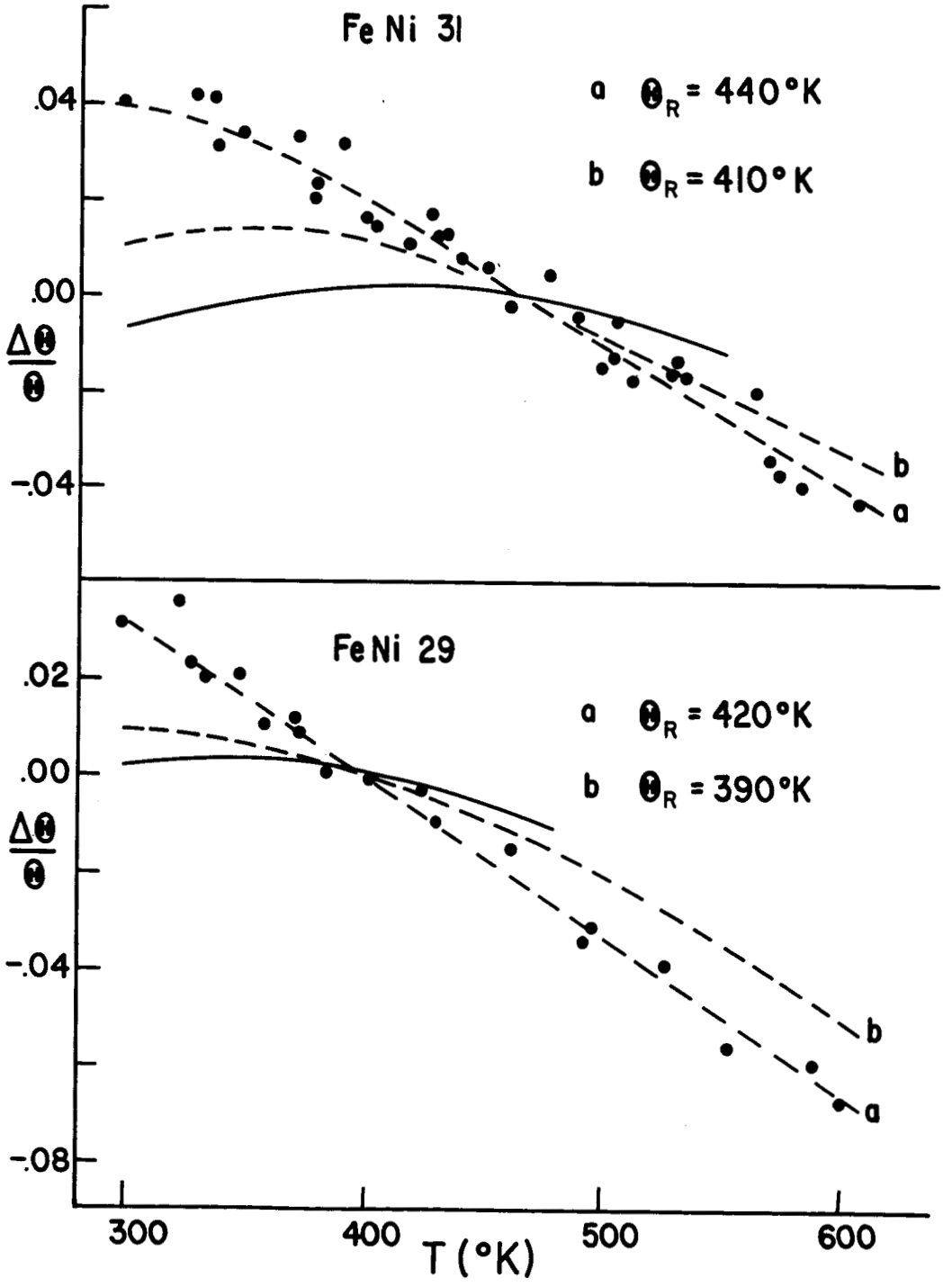
Fe Ni 31
a Θ_R = 440°K
b Θ_R = 410°K
.04
.00
-.04
$\frac{\Delta\Theta}{\Theta}$
b
a
Fe Ni 29
a Θ_R = 420°K
b Θ_R = 390°K
.02
.00
-.04
-.08
$\frac{\Delta\Theta}{\Theta}$
b
a
300
400
500
600
T (°K)

SECTION VI

DISCUSSION OF RESULTS

The difference in the temperature dependence of the Debye temperature determined from ultrasonic measurements and x-ray measurements must de discussed in terms of the essential differences in the measuring process. The ultrasonic measurements were made by applying a stress at frequencies of about $(10)^7$ cycles per second. The x-ray results are determined by the displacements of atoms from their equilibrium positions due to thermal vibrations; these displacements are determined by thermal waves having fequencies over a range around $(10)^{12}$ cycles per second. Therefore, any contribution to the elastic constants which contributes in one of these frequency ranges and not the other would cause a difference in the Debye temperature determined by the two methods. Furthermore, any stress induced contributions in the ultrasonic measurements would not be measured by the x-ray techniques since the x-ray measurements are virtually stressless.

It is also necessary to discuss the nature of the magnetic effects in order to interpret our observations. In part A the nature of the magnetic effects will be discussed. Then in part B, the difference between the x-ray and the ultrasonic $\frac{\Delta\Theta}{\Theta}$ versus T curves will be discussed.

A. Magnetic Effects

The theory of magnetic exchange interactions which lead to

coupling between the magnetic moments of atoms in a crystal has recently been reviewed by Anderson (P. W. Anderson, 1963). He states that "it can be fairly said that most of the mechanisms in insulators are at least qualitatively, and sometimes quantitatively, understood, while the exchange question in metals is still almost completely open." Nevertheless, the concept of an exchange energy is frequently used in the discussion of the ferromagnetism of metals and alloys. It is of the form (P. W. Anderson, 1963, p. 101):

$$V = -\sum_{ij} J_{ij}\ \underline{S}_i \cdot \underline{S}_j \qquad 6.1$$

where J_{ij} is the exchange integral between electrons and $\underline{S}_i$ is the spin of the ith electron. This is the basis of an interatomic exchange energy J (Bethe, 1933) which is shown in Figure 8 as a function of interatomic distance normalized to the radius of the d electron shell. This energy can be related to the Curie temperature of ferromagnetic elements and used to qualitatively place the elements on the curve in Figure 8 (Bozorth, 1951, p. 444). In the case of a disordered alloy such a procedure is not possible because different pairs of atoms would have different exchange energies and would fall on different portions of the curve. This point of view is adopted by Kondorsky and Sedov (1960) and by Kouvel and Wilson (1961) in interpreting their measurements of the large pressure dependence of magnetization in iron-nickel alloys of 30 to 50 percent nickel. The placement of the different interactions in Figure 8 is

Figure 8

Bethe-Slater Curve

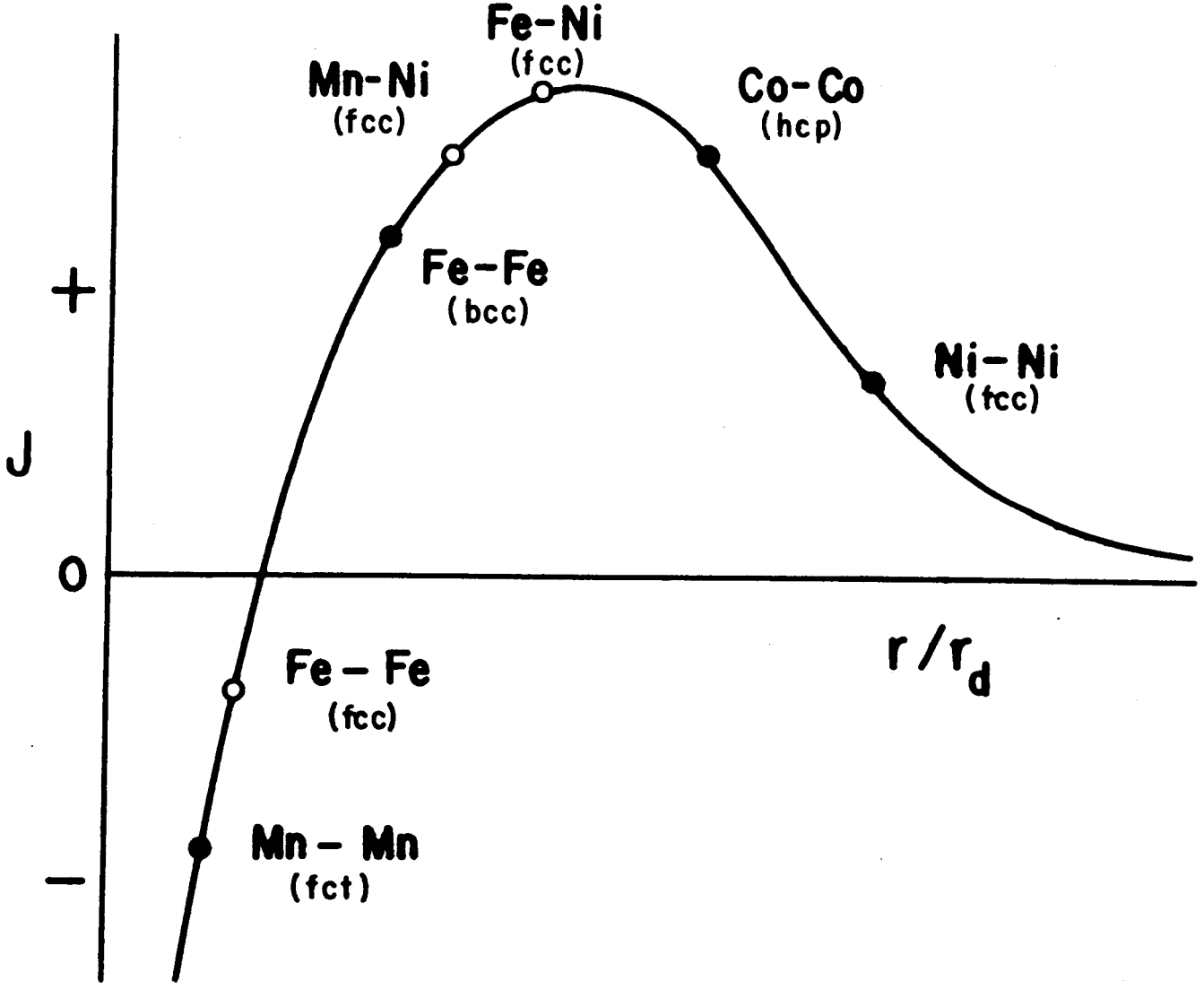
Fe-Ni
(fcc)
Mn-Ni
(fcc)
Co-Co
(hcp)
Fe-Fe
(bcc)
Ni-Ni
(fcc)
+
J
0
r/r_d
Fe-Fe
(fcc)
Mn-Mn
(fct)
−

taken from Kouvel and Wilson. In particular notice that the iron-iron interaction in a face-centered-cubic lattice is taken as negative. This leads to the possibility that some iron atoms may have a very small or even a net negative J value for some environment of nearest neighbors. As we have indicated, the meaning of such an interatomic exchange energy in metals is not clear on theoretical grounds. Qualitatively it seems justifiable in explaining the pressure dependence of the magnetization in the alloys under discussion. Furthermore, ANS (Alers, Neighbors and Sato, 1960) have used it successfully in analyzing their ultrasonic measurements on these alloys. They introduce the elastic energy as

$$E = E_o - \frac{1}{2} N z \left(\frac{I}{I_o}\right)^2 J(r) \qquad 6.2$$

where J(r) is the interatomic magnetic exchange energy, I/I_o the relative magnetization, z the number of nearest neighbors, N the number of atoms per unit volume and E_o the collection of all energies not related to the alignment of magnetic moments.

The second term in equation 6.2 is an obvious analogy with equation 6.1 with Bethe's concept of interatomic exchange substituted for the electronic exchange integral. From equation 6.2 ANS write for the two shear modulii and the bulk modulus

$$C_I = [c_{44}]_I = C_o - \frac{N}{2}\left(\frac{I}{I_o}\right)^2 \left(r_e^2 \frac{d^2J}{dr^2} + 3 r_e \frac{dJ}{dr}\right) \qquad 6.3$$

$$C_I' = \left[\frac{1}{2}(C_{11}-C_{12})\right]_I = C_o' - \frac{N}{4}\left(\frac{I}{I_o}\right)^2\left(r_e^2\frac{d^2J}{dr^2} + 7r_e\frac{dJ}{dr}\right) \qquad 6.4$$

$$B_I = \left[\frac{1}{3}(C_{11}+2C_{12})\right]_I = B_o - \frac{2N}{3}\left(\frac{I}{I_o}\right)^2 r_e^2\frac{d^2J}{dr^2} \qquad 6.5$$

where the subscript I denotes constant magnetization and the subscript 0 denotes the value in the absence of ferromagnetism. The equilibrium interatomic distance is denoted by r_e. These magnetic terms are consistent with Fuch's (1936) expressions for nearest neighbor interactions in face-centered-cubic materials.

In their discussion they assume that

$$\frac{1}{B_I} = \frac{1}{B_H} - \frac{w^2}{dI/dH} \qquad 6.6$$

which is important since the measurements are actually made at constant magnetic field, H, and not at constant magnetization. The second term on the right side of equation 6.6 is the so-called Döring term in which the magnetization is changed by the applied stress through the volume magnetostriction, $w = \frac{d\upsilon}{dH}$.

On the other hand they argue that $C_I = C_H$ and $C_I' = C_H'$ since "it is a known fact that shearing distortions (spontaneous morphic magnetostriction), which result from a change in the spontaneous magnetization, are small compared to the accompanying volume distortions (spontaneous volumemagnetostriction)."

From their measurements ANS conclude that

$$\frac{N}{2} r_e \frac{dJ}{dr} = (+7 \pm 2)\ (10)^9 \quad \frac{dyne}{cm^2}$$

and

$$\frac{N}{2} r_e^2 \frac{d^2J}{dr^2} = (-15 \pm 9)\ (10)^9 \quad \frac{dyne}{cm^2}$$

for their iron-nickel alloy.

On the basis of these values essentially all of the magnetic effect in B is due to the Döring term. ANS could not calculate the value of the Döring term because they did not know the value of dI/dH. In appendix E we derive a different expression for the Döring term which can be calculated from available data. The values calculated are consistent with the entire magnetic effect in B being due to the Döring term. To see the effect of the Döring term on the Debye temperature we remove the Döring term from B and give B a negative temperature slope of 1.4 $(10)^{-7}$ per C°. The resulting $\frac{\Delta\Theta}{\Theta}$ versus T curve can be seen in curve b in Figure 9. This is to be compared with curve a in which all of the magnetic effects measured ultrasonically have been included.

The large uncertainties given by ANS for their values quoted above come principally from the uncertainty in the volume dependence of C and C'. This volume dependence causes some of the observed change in slope due to the change in thermal expansion below the Curie temperature. As discussed in appendix C it is pos-

Figure 9

Effect of Removing Different Magnetic Contributions
in the Debye Temperatures Versus Temperature
Calculated from Elastic Constants

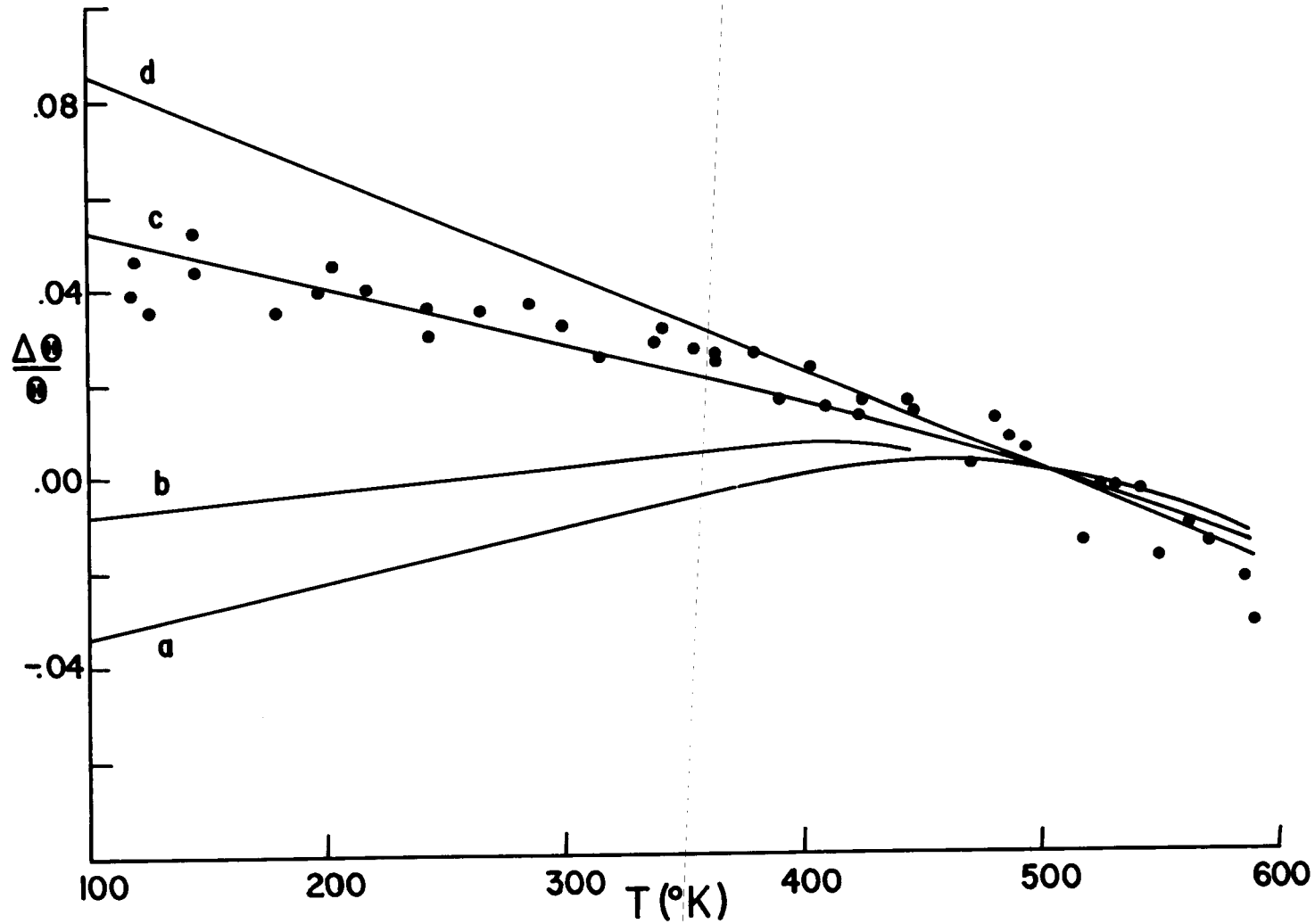
d
c
b
a
.08
.04
.00
-.04
$\frac{\Delta\Theta}{\Theta}$
100
200
300
400
500
600
T (°K)

sible to attribute all of the observed change in slope in C versus T to this volume dependence. In fact it is argued there that this much volume dependence is to be expected in C. For C' the volume dependence is expected to be much less; moreover, even a large volume dependence of C' could not account for the positive slope observed. Therefore, we attribute most of the change in slope of C versus T to the volume dependence of C; we attribute most of the change in slope in C' versus T to the magnetic term in equation 6.4. This is consistent with the ANS results for dJ/dr and d^2J/dr^2.

To see the effects of these two factors on the Debye temperature calculated from the elastic constants we have removed the magnetic effect from C' and given C' a negative slope of $7\ (10)^{-7}$ per C° in curve c of Figure 9. This leaves only the effects in C to cause the change in slope in curve c; therefore, the change in slope in curve c can be considered as being due to volume effects alone.

Curve d in Figure 9 is an extension of the high temperature slope of curve c. The data points in Figure 9 are for the 33 percent sample with $\Theta_R = 430°K$.

B. Interpretation

From the preceeding discussion we see that there are three distinguishable effects which contribute to the change in slope of the $\frac{\Delta\Theta}{\Theta}$ versus T curves calculated from the ultrasonic elastic constants. One is the stress induced Döring term. Another is the so-

called "intrinsic" magnetic effect introduced by ANS and shown in equations 6.3 - 6.5. The third is the dependence of the elastic constants on volume which is only indirectly due to magnetic effects through the change in slope of lattice constant versus temperature. The approximate effect of successively removing these effects from the elastic constants has been shown successively in going from curve a to b to c to d in Figure 9.

First let us consider whether or not the Döring term would be expected to contribute to the x-ray measurements. It is due to stress induced changes in the magnetization which can be attributed to a dependence of J on interatomic distance. Therefore, it should not be present in the stressless x-ray measurements. It is argued by ANS that a similar effect does not exist in C and C' because there is no volume strain involved in these shear distortions and because the spontaneous morphic magnetostriction is small. However, in a disordered alloy these arguments are not entirely valid. The effect on C and C' can exist in a disordered alloy because a net change in J for a given atom can take place in a shearing strain if the nearest neighbors involved in the shearing strain about the atom have a different value of dJ/dr. This change could cause the reversal in the magnetic moment of some atoms and by statistical arguments involving the relative number of atoms in a given environment there could be a net change in magnetization so that the assumption, $C_I = C_H$ and $C'_I = C'_H$ used by ANS would not necessarily be valid.

However, such an argument could not predict the observed difference in the size of the magnetic effect in C and C' without using some rather unfounded assumptions. Therefore, it does not seem reasonable to attribute the observed magnetic effects in these shear strains to stress induced magnetization changes. In fact, it is difficult to explain the difference in the size of the magnetic contribution in C and C' without invoking equations 6.3 and 6.4 as used by ANS.

Turning now to the volume dependence of the elastic constants we argue that this effect should certainly appear in the x-ray measurements since it is due to the volume dependence of the non-magnetic terms in equations 6.3 - 6.5 and does not depend on the nature of the magnetic effects. We see in Figure 9 that the data for one choice of Θ_R for the 33 percent alloy fits curve c reasonably well. Thus, it is possible to attribute the observed change in slope in the x-ray data for $\frac{\Delta\Theta}{\Theta}$ versus T to the volume effect alone.

Apparently the effects present in curve b of Figure 9 which are due to the magnetic effects in C' do not appear in the x-ray data. Since we could not ascribe these contributions to C' to stress induced effects then we must consider them as being frequency dependent in order to explain the difference between the x-ray and ultrasonic results.. To estimate the effect of such a frequency dependence we have developed a simple model in appendix D to treat a frequency dependent magnetic contribution to the elastic constants. It serves two functions. First, it shows that fre-

quency dependent elastic constants cannot account for a large negative curvature in the Θ versus T data. Therefore, it cannot be argued that a lower Θ_k value which gives such a curvature could have been chosen. Second, it allows an estimate of the highest frequency at which the magnetic effects could contribute to the elastic constants. Using this model and comparing the data in Figure 9 with curve c we estimate that the intrinsic magnetic effects could not be contributing at frequencies higher than one-tenth of the Debye frequency. In the extreme case of allowing no volume dependence of the elastic constants we compare the data with curve d and estimate that the intrinsic magnetic effects could not contribute at more than three-tenths of the Debye frequency.

SECTION VII

CONCLUSIONS

Reviewing the situation as presented in the last section we see that it seems necessary to use an interatomic exchange energy, J, in order to explain the ultrasonic elastic constant measurements of ANS on an alloy of 30 percent nickel in iron. The meaning of such an energy is not clear from the theory of ferromagnetism in metals. This is especially true in the case of a disordered alloy such as the one measured by ANS. There is evidence to indicate that the different elements in this alloy can have widly differing values of J. In that case a single value of J appropriate for use in equation 6.2 must represent some sort of average of the different interatomic exchange energies.

It is possible for this averaging process to be inherent in the nature of the ferromagnetic interactions. This would imply some sort of long range ferromagnetic interaction. Such long range interactions have been postulated (see Paskin, 1960 and the references therein) but are not established experimentally.

Alternatively, one might describe the averaging as being some sort of spatial average over the wavelength of the ultrasonic wave. This would be an average performed by the measuring process.

However, our x-ray data indicate that the magnetic effects in equations 6.3 - 6.5 are not present in the high frequency, short wavelength processes involved in the x-ray measurements. Thus, we

infer that the averaging processes discussed above do not occur under these conditions.

If the averaging is due to long range ferromagnetic interactions we can conclude that the interactions do not respond at these frequencies.

If the averaging is over the wavelength of the vibrational waves we conclude that random fluctuations in composition make the average meaningless for very short wavelengths.

In any case, we conclude that our x-ray data support the point of view that, although the magnetic effect in the elastic constants is <u>not</u> due to an intrinsic contribution to the elastic energy of the kind propsed by ANS, the concept of some averaged magnetic contribution to the elastic energy is useful in explaining their ultrasonic measurements.

SECTION VIII

SUMMARY

We have developed a technique for measuring the intensity of Bragg peaks reflected from the face of a large single crystal over a range of temperatures from 100°K to 600°K. An expression for correcting the measured intenstities for diffuse scattering has been developed.

These techniques have been used on nickel and iron-nickel alloys to obtain the temperature dependence of the x-ray Debye temperature for these materials. This temperature dependence has been compared with the temperature dependence of the Debye temperature calculated from ultrasonic elastic constant measurements. In the case of the alloys the difference has been interpreted in terms of the nature of the magnetic effect in the elastic constants.

It is felt that there are other materials where meaningful comparisons of this type can be made. This is especially true where the ultrasonic and x-ray measurements can be made on the same sample. Our x-ray techniques are suitable for this purpose.

SECTION IX

APPENDICIES

APPENDIX A: Correction for Diffuse Scattering

It has long been recognized that the thermal motion which causes the decrease in Bragg intensities in x-ray scattering gives rise to background scattering known as the thermal diffuse scattering. The basis for an analysis of this effect has been given in Section III; the diffuse scattering is discussed there briefly. In equation 3.17 I_2 can be thought of as the scattering out of the Bragg peak due to the absorption or emission of one phonon during the scattering process. This scattering produces a diffuse peak under the Bragg peak. The higher order terms are due to multi-phonon processes and contribute to the general background with no significant peaking. Therefore, we will be concerned only with I_2 since it may contribute significantly to the measured intensity. I_2 must then be subtracted from the measured intensity in order to obtain the true integrated intensity of the Bragg peak.

This contribution has been recognized for some time, but only relatively recently have corrections been applied for it. Chipman and Paskin (1959) have derived a scheme for correcting for this effect in polycrystaline measurements. Nilsson (1957) has derived a method for correcting single crystal measurements for an omega or moving crystal, fixed counter scan assuming no mosaic spread in the crystal. Neither of these were applicable to the procedures used by us. Therefore, it was necessary to develop a method for cor-

recting our measurements for diffuse scattering.

The approximations we have used are similar to those of Nilsson: first averaging the scattering over all directions in reciprocal space and treating the average isotropically; then considering the counter window to have infinite height and allowing the background subtraction to compensate for the approximation. We have, however, improved on his method by allowing for the effects of mosaic spread and beam divergence. In addition, we have introduced a simpler scheme for the directional averaging which will allow easier analytical comparison with the Debye-Waller factor.

We modify our notation of Section III by using j instead of I to indicate the scattering per unit solid angle. Then

$$j_1 = F^2 e^{-2M} \sum_n \sum_m e^{i\kappa \underline{S}\cdot(\underline{r}_n - \underline{r}_m)} = F^2 e^{-2M} \; Y(\kappa \underline{S}) \qquad A\text{-}1$$

is the Bragg intensity and

$$j_2 = F^2 e^{-2M} \sum_{k_j} G_{k_j} \sum_n \sum_m e^{i\kappa \underline{S}\cdot(\underline{r}_n - \underline{r}_m)} \cos\left[\underline{k}\cdot(\underline{r}_n - \underline{r}_m)\right]$$

$$= F^2 e^{-2M} \sum_{k_j} G_{k_j} \tfrac{1}{2}\left[Y(\kappa \underline{S} - \underline{k}) + Y(\kappa \underline{S} + \underline{k})\right] \qquad A\text{-}2$$

is the first order diffuse intensity. Here we have introduced the interference function $Y(\kappa \underline{S})$ which is sharply peaked at $\underline{S} = \underline{S}_0$. We now replace the summation over k by an integration over k space

using $dN = \frac{Nq^3}{(2\pi)^3} dk_x\, dk_y\, dk_z$. We are interested in the value of j_2 at a fixed value of $\underline{S}$ so the integration is performed at constant $\underline{S}$. The interference function is non-zero only at values of k such that $\hbar\underline{S} + \underline{k} = \hbar\underline{S}_o$. Therefore, the value of G_{kj} at this value of k is the only significant contribution. The integration over the interference function gives $N(2\pi)^3/a^3$ so we have

$$j_2(\underline{k}) = F^2 e^{-2M} N^2 \sum_j G_{kj} \qquad A\text{-}3$$

For $kT \gg \hbar\omega_{kj}$ which is valid near the Bragg peak at temperatures where the diffuse scattering is significant, we can write from equation 3.12

$$G_{kj} = \frac{\hbar}{m\eta} \frac{(\hbar\underline{S}\cdot\underline{e}_{kj})^2 (n_{kj}+\frac{1}{2})}{\omega_{kj}}$$

$$\simeq \frac{kT}{m\eta} \frac{1}{\omega_{kj}^2} (\hbar\underline{S}\cdot\underline{e}_{kj})^2 \qquad A\text{-}4$$

Then introducing the velocity of the thermal waves $v_{kj} = \frac{\omega_{kj}}{k}$ we get

$$G_{kj} = \frac{kT}{m\eta} \frac{1}{k^2} \frac{(\hbar\underline{S}\cdot\underline{e}_{kj})^2}{v_{kj}^2} \qquad A\text{-}5$$

Then

$$j_2 = F^2 e^{-2M} \frac{kT}{m} \frac{N^2}{\eta} \frac{1}{k^2} \sum_j \frac{(k\underline{S}\cdot\underline{e}_{kj})^2}{v_{kj}^2} \qquad A\text{-}6$$

At this point we will take the isotropic average by setting

$$\left[(k\underline{S}\cdot\underline{e}_{kj})^2\right]_{\substack{\text{averaged over}\\ \text{all directions}}} = \frac{k^2S^2}{3} = \frac{16\pi^2\sin^2\theta}{3\lambda^2} \qquad A\text{-}7$$

Then using

$$v_j^2 = \frac{\mu_j}{\rho} = \frac{\mu_j a^3}{\nu m} \qquad A\text{-}8$$

where μ_j is the isotropic elastic constant of the jth mode and ν is the number of atoms per unit cell. Noting that $\frac{N}{\eta} = \frac{1}{\nu}$, we can write

$$j_2 = F^2 e^{-2M} \frac{4NkT}{3a^3} \frac{\sin^2\theta}{\lambda^2} \frac{4\pi^2}{k^2} \sum_j \frac{1}{\mu_j} \qquad A\text{-}9$$

This is the diffuse scattering into an elemental solid angle for a given crystal setting.

Using an Ewald sphere of radius $2\pi/\lambda$, we now construct a co-ordinate system in reciprocal space which is centered at a Bragg peak as illustrated in Figure 10. For small distances from the Bragg peak the co-ordinates represent angular motions of the diffraction apparatus so that distances in reciprocal space are $2\pi/\lambda$

Figure 10

Angular Co-ordinates Relative
to the
Ewald Sphere

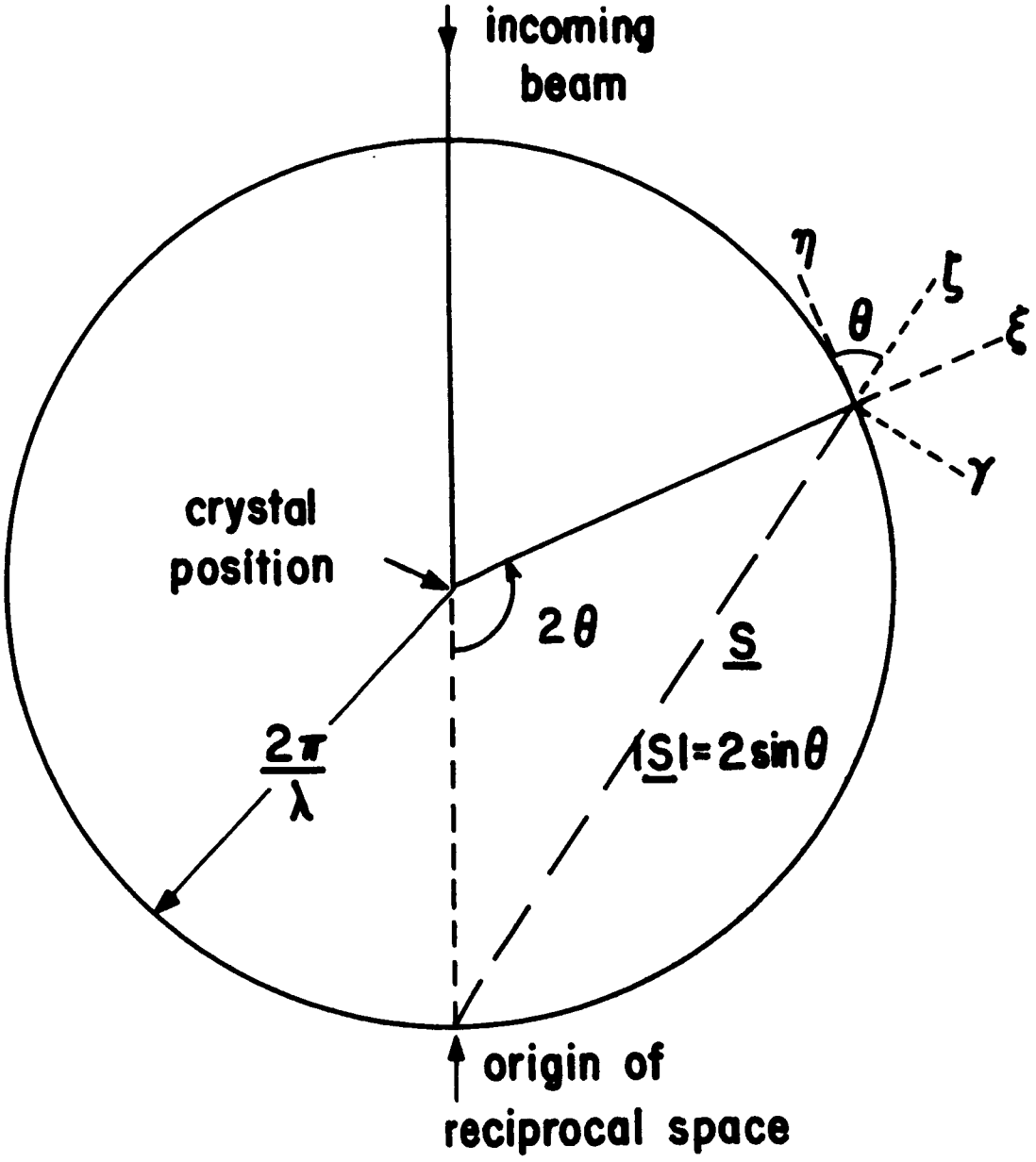
incoming
beam
η
ζ
θ
ξ
γ
crystal
position
2θ
S
|S|=2sinθ
2π
λ
origin of
reciprocal space

times the co-ordinated angle.

As shown in Figure 10, γ corresponds to a rotation of the crystal about the normal to the page such that $\gamma = 2\sin\theta(\omega - \omega_o)$ where ω is the true angular rotation of the crystal. ζ corresponds to the usual 2θ motion of a diffractometer such that $\zeta = (2\theta - 2\theta_o)\cos\theta$. η corresponds to a counter rotation or the counter slit width. ξ is the motion perpendicular to η. The direction normal to the page is the χ motion of the G. E. goniostat which corresponds to rotation out of the plane of diffraction or to the counter slit height. These form two orthogonal systems rotated about χ by an angle θ.

To obtain the intensity of diffuse scattering collected at any given counter setting we must integrate j_2 over the solid angle subtended by the counter window.

$$i_2' = \int_{\Delta\eta}\int_{\Delta\chi} j_2 \, d\eta \, d\chi \qquad A\text{-}10$$

Similarly for j_1

$$i_1' = \int_{\Delta\eta}\int_{\Delta\chi} j_1 \, d\eta \, d\chi \qquad A\text{-}11$$

However, for a real crystal there is a range of angles for which a crystal reflects because of the mosaic nature of the crystal. This necessitates that the intensity scan cover this range; it also means that the diffuse intensity at a given setting of the counter

is an average over this range. A satisfactory approximation for this is to average i_2' over a step function whose width, $\Delta\xi$, is the full ξ width of the Bragg peak at one-half intensity. Using $k^2 = \left(\frac{2\pi}{\lambda}\right)^2(\xi^2 + \eta^2 + \chi^2)$ this gives

$$i_2 = \frac{\int_{\Delta\xi} i_2' \, d\xi}{\Delta\xi} = F^2 e^{-2M} \frac{N}{a^3} \frac{4\pi^4 T}{3} \frac{\sin^2\theta}{\lambda^2} \left(\sum_j \frac{1}{\mu_j}\right) \beta \qquad A\text{-}12$$

where

$$\beta = \frac{1}{\pi \Delta\xi} \int_{\Delta\xi} \int_{\Delta\eta} \int_{\Delta\chi} \frac{d\chi \, d\eta \, d\xi}{(\xi^2 + \eta^2 + \chi^2)} \qquad A\text{-}13$$

Thus at any given setting the intensity is

$$i = i_1 + i_2 + i_c \qquad A\text{-}14$$

where i_c is a constant background contribution.

The total count $\mathcal{E}$ for a 2θ scan after background subtraction is

$$\mathcal{E} = \int i_1 \frac{d(2\theta)}{\Omega} + \int i_2 \frac{d(2\theta)}{\Omega} + \int i_c \frac{d(2\theta)}{\Omega} - i_c \frac{\delta(2\theta)}{\Omega} - i_{2b} \frac{\delta(2\theta)}{\Omega} \qquad A\text{-}15$$

where Ω is the angular velocity of the scan and $\delta(2\theta)$ is the range of the scan. The scan starts and ends where i_1 is zero, so its limits of integration may be extended throughout the zone of reciprocal space. Then

$$\mathcal{E}^{o} = \frac{F^2 e^{-2M}}{\sin\theta\cos\theta}\,\frac{\lambda^3 N}{a^3}\,\frac{1}{\Omega} + + F^2 e^{-2M}\,\frac{N}{a^3}\,\frac{4\pi R T}{3}\,\frac{\sin^2\theta}{\Omega}\left(\sum_j \frac{1}{\mu_j}\right)\left[\int_{\delta(2\theta)} \beta\, d(2\theta) - \beta_0\,\delta(2\theta)\right]$$

$$= \frac{F^2 e^{-2M}}{\sin\theta\cos\theta}\,\frac{\lambda^3 N}{a^3}\,\frac{1}{\Omega}\left[1 + \frac{\sin^3\theta}{\lambda^3}\cos\theta\,\frac{4\pi R T}{3}\left(\int \beta\, d(2\theta) - \beta_0\,\delta(2\theta)\right)\sum_j \frac{1}{\mu_j}\right]$$

$$= \mathcal{E}_1^{o}\left[1 + \alpha\right] \qquad \text{A-16}$$

By dividing the observed intensity by $1 + \alpha$ one then obtains the integrated count for the Bragg intensity $\mathcal{E}_1$.

To evaluate α we need

$$\sum_j \frac{1}{\mu_j} = \frac{1}{E} + \frac{2}{\mu} \qquad \text{A-17}$$

This can be calculated in one of three ways: directly from the polycrystaline elastic constants - Youngs modulus, E, and the shear modulus, μ; calculated from the single crystal elastic constants, by the method similar to Anderson's (1963); or estimated from some knowledge of the Debye temperature. For our work we used the elastic constant data of ANS and the method of Anderson.

Integrating to get β we used the limits $-\infty$ to $+\infty$ for χ; $\eta_1 = \zeta\cos\theta - \frac{\Delta\eta}{2}$ to $\eta_2 = \zeta\cos\theta + \frac{\Delta\eta}{2}$ for η; and $\xi_1 = \zeta\sin\theta - \frac{\Delta\xi}{2}$ to $\xi_2 = \zeta\sin\theta + \frac{\Delta\xi}{2}$ for ξ, to get

$$\beta = \xi_2\left[\ln\left(\eta_2+\sqrt{\eta_2^2+\xi_2^2}\right)-\ln\left(\eta_1+\sqrt{\eta_1^2+\xi_2^2}\right)\right]+$$

$$+\xi_1\left[\ln\left(\eta_1+\sqrt{\eta_1^2+\xi_1^2}\right)-\ln\left(\eta_2+\sqrt{\eta_2^2+\xi_1^2}\right)\right]$$

$$+\eta_2\left[\ln\left(\xi_2+\sqrt{\eta_2^2+\xi_2^2}\right)-\ln\left(\xi_1+\sqrt{\eta_2^2+\xi_1^2}\right)\right]$$

$$+\eta_1\left[\ln\left(\xi_1+\sqrt{\eta_1^2+\xi_1^2}\right)-\ln\left(\xi_2+\sqrt{\eta_1^2+\xi_2^2}\right)\right] \qquad \text{A-18}$$

We define

$$\sigma = \cos\theta\left[\int_{\delta(2\theta)}\beta\, d(2\theta)-\beta_b\,\delta(2\theta)\right]=\int_{\delta(\zeta)}\beta\, d\zeta-\beta_b\,\delta(\zeta) \qquad \text{A-19}$$

The expression for β is numerically integrated to calculate σ. The values of β at the background counting positions are averaged in order to obtain β_b.

The other factors are straightforward. The values of α for our work are illustrated in appendix B along with other correction factors.

APPENDIX B: Correction for the Change in Lattice Constant and Numerical Values for the Total Correction

We shall here develop the expressions for the minor corrections to be applied to the integrated intensities in order to take into account the dependence of the integrated intensity on the lattice parameter due to the change of lattice parameter with temperature. These corrections along with the diffuse scattering correction from appendix A will be illustrated in detail for nickel. The corrections for the other samples were obtained by the same procedure and gave similar numerical values.

The integrated intensity from the face of a large mosaic crystal is (James, 1954, ch. 2)

$$I(T) = \frac{J\eta^2\lambda^3}{2\mu}\left(\frac{e^2}{m_e c^2}\right)^2 \frac{1+\cos^2 2\theta_o}{\sin 2\theta_o}\left|\sum_n f_n e^{2\pi i(hx_n+ky_n+lz_n)}\right|^2 e^{-2M(T)}$$

$$= I_o(T)\ e^{-2M(T)} \qquad \text{B-1}$$

where J is the incident x-ray intensity, λ is the x-ray wavelength, e is the electronic charge, c the velocity of light, m_e is the mass of an electron, η is the number of atoms per unit volume, which is proportional to $1/a^3$ where a is the lattice parameter, μ is the linear absorption coefficient which is proportional to $1/a^3$, f_n is the atomic scattering factor for the nth atom in the unit cell and θ_o is the Bragg angle which is related

to a by

$$\sin\theta_o = \frac{\lambda\sqrt{h^2+k^2+l^2}}{2a}$$

where h, k and l are the Miller indicies of the Bragg reflection.

If $\Delta a = a(T) - a(T_R)$ is small, then

$$\Delta\left(\frac{1+\cos^2 2\theta_o}{\sin 2\theta_o}\right) = \frac{1+\cos^2 2\theta_o}{\sin 2\theta_o}\left(\frac{4\cos 2\theta_o \sin 2\theta_o}{1+\cos^2 2\theta_o} + \right.$$

$$\left. + \frac{2\cos 2\theta_o}{\sin 2\theta_o}\right)\tan\theta_o \frac{\Delta a}{a}$$

$$= \frac{1+\cos^2 2\theta_o}{\sin 2\theta_o}\epsilon_1 \frac{\Delta a}{a} \qquad B\text{-}2$$

and

$$\Delta\left(\frac{N^2}{\nu}\right) = \frac{N^2}{\nu}(-3)\frac{\Delta a}{a} \qquad B\text{-}3$$

and

$$\Delta(f^2) = f^2\left(-\frac{2}{f}\frac{df}{d\left(\frac{\sin\theta}{\lambda}\right)}\right)\frac{\sin\theta}{\lambda}\frac{\Delta a}{a}$$

$$= f^2\epsilon_2\frac{\Delta a}{a} \qquad B\text{-}4$$

Then

$$I_o(T) = I_o(T_R)\left[1 + (\epsilon_1 + \epsilon_2 - 3)\frac{\Delta a}{a}\right]$$

$$= I_o(T_R)\left[1 + \epsilon\ \frac{\Delta a}{a}\right] \qquad B\text{-}5$$

which is a correction which will allow us to treat I_o as a constant.

In addition there is a similar correction in the exponent

$$2M = A\,\frac{1}{\Theta}\left\{\frac{\phi(x)}{x} + \frac{1}{4}\right\} = A\,\psi \qquad B\text{-}6$$

But A is proportional to $\sin^2\theta$ which is proportional to $1/a^2$ so that

$$A(T) = A(T_R)\left[1 - 2\,\frac{\Delta a}{a}\right] \qquad B\text{-}7$$

and

$$e^{-A(T)\,\psi} = e^{-A(T_R)\psi}\, e^{2A\psi\frac{\Delta a}{a}}$$

$$\cong \left(1 + 2A\psi\,\frac{\Delta a}{a}\right) e^{-A(T_R)\,\psi} \qquad B\text{-}8$$

which is a correction which allows us to treat A as a constant.

Finally, applying all these corrections plus the diffuse scattering correction to the measured intensities we get

$$I_c(T) = \frac{I_m(T)}{(1+\alpha)\left(1+\epsilon\frac{\Delta a}{a}\right)\left(1+2A\psi\frac{\Delta a}{a}\right)}$$

$$= I_o(T_R)\; e^{-A(T_R)\,\psi} \qquad B-9$$

If all these corrections are small, as they are in our case, then they can be combined into a single factor, $\alpha + (\epsilon + 2A\psi)\,\Delta a/a$, which represents a fractional decrease in the measured intensity.

The corrections for the change in lattice parameter are straightforward calculations from a knowledge of f, $A\psi$, θ_o and of a versus T. The $A\psi$ values can be obtained from the uncorrected experimental data. For our calculations the atomic scattering factors as calculated by Freeman and Watson (1961) were used. A weighted average of their iron and nickel values was used for the alloys.

To calculate α we have from appendix A

$$\alpha = \frac{4\pi k}{3}\,\frac{\sin^3\theta_o}{\lambda^3}\left(\sum_j \frac{1}{\mu_i}\right)\left(\int_{\delta S} B\,dS - B_b\,\delta S\right)T$$

$$= \frac{4\pi k}{3}\,\frac{\sin^3\theta_o}{\lambda^3}\,k\,\sigma\,T \qquad B-10$$

The value of κ was determined from the same elastic constant calculations as were used to calculate the Debye temperatures. Using Anderson's (1963) notation we have

$$\kappa = \frac{1}{B + \frac{4}{3}\mu_H} + \frac{2}{\mu_H}$$

For nickel at room temperature $\kappa = 2.656\ (10)^{-12}$ cm^2/dyne.

In the case of the (660) peak of nickel the separation of the K_{α_1} and K_{α_2} peaks is 1.14 degrees in 2θ. Therefore, the 2θ scan was from an angle below the K_{α_1} peak to 1.14 degrees plus that angle above it so that the scan was symetrical with respect to the K_{α_1} and K_{α_2} peaks and the same σ value was applicable to both peaks. For the nickel sample the scan started 1.00 degrees below the K_{α_1} peak so that the total scan range was $\delta(2\theta) = 3.14$ degrees.

The parameters needed for calculating β are

$$\Delta\xi = \Delta\gamma \cos\theta = \Delta\omega \sin 2\theta = .60 \sin 118^\circ = .26$$

$$\Delta\eta = 1.20$$

Then to get σ we numerically integrate β between the limits

$$\xi_1 = -1.00 \cos 59^\circ = -.51$$

$$\xi_2 = 2.14 \cos 59^\circ = 1.10$$

to get

$$\int_{\zeta_1}^{\zeta_2} \beta \, d\zeta = .0859$$

Then using

$$\beta_b = \frac{\beta_{.51} + \beta_{1.10}}{2} = .0298$$

and

$$\delta\zeta^\circ = 3.14 \cos 59^\circ = 1.61$$

we have

$$\sigma = .0859 - .0477 = .0382$$

and for room temperature

$$\alpha = (5.78\,(10)^{-16})(1.763\,(10)^{24})(2.656\,(10)^{-12})(.0382)(300) = .030$$

The values of α versus T calculated for the (660) peak of nickel are shown in Figure 11.

For the (660) peak of nickel

Figure 11

Intensity Correction Parameters

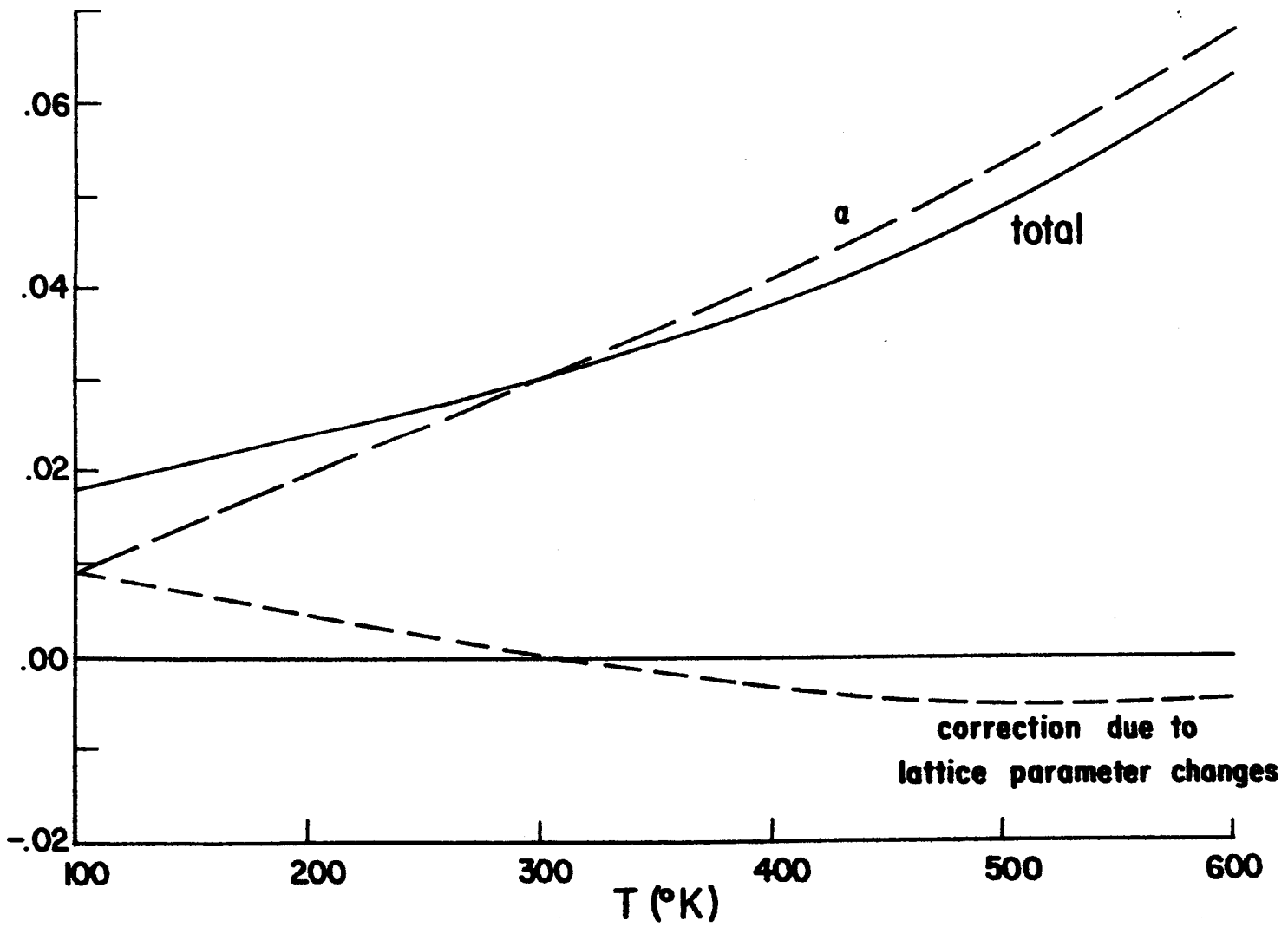
.06
.04
.02
.00
-.02
α
total
correction due to
lattice parameter changes
100
200
300
400
500
600
T (°K)

$$\epsilon = (\epsilon_1 + \epsilon_2 - 3) = (-4.0 + 1.4 - 3) = -5.6$$

Using the observed $A\psi$ and $\Delta a/a$ we calculate the values shown in Figure 11 for the lattice parameter corrections. The sum of the two corrections which represents the total correction is also shown in Figure 11.

APPENDIX C: Adjustment of Elastic Constants for Composition Changes

As indicated in Section V the composition of our alloys was different from that of the alloy measured by ANS. To find the appropriate behavior of the elastic constants of our alloys it is necessary to shift the break in the slope according to the location of the Curie temperature for each alloy. In addition there is the possible composition dependence of the size of the change in slope. The shift in Curie temperature is determined by the observed lattice parameter versus temperature curves and is accomplished quite accurately. The largest composition change is about 2 percent for the 33 percent sample based on the shift in Curie temperature. Available data from the literature are used to show that the composition dependence of the magnetic effect is small in this composition range so that the size of the change in slope of B and C' is quite justifiably kept constant for all samples. For C it is shown that the observed change in slope is nearly all due to the change in slope of a versus T. This is consistent with the magnetic effects and with the temperature dependence of C in other materials. Therefore, the change in slope of C for the different compositions was determined from the observed a versus T.

To determine the shift in Curie temperatures for each alloy the Curie temperature of our samples were measured by an AC susceptibility method on apparatus made available to us by Carl

Rosner of the General Electric Research Laboratory. For the 29, 31 and 33 percent samples the Curie temperatures are 367, 438, and 466°K, respectively. Then using strictly empirical arguments, we compared these with the extrapolated intersection of the $4a/a$ versus T curves of Figure 5. The location of these intersections is certainly related to the Curie temperature since the curvature of these curves is due to the magnetic effects. These intersections are 45, 36, and 35 degrees less than the respective Curie temperatures. The intersection of the curve for the ANS sample is 365°K. This is about half way between the 29 and 31 percent samples, so we estimated that the Curie temperature for their sample is 41 degrees above 365°K, i.e. 406°K. This value is lower than that estimated by ANS but it is not inconsistent with their data and should be within 5 degrees of the Curie temperature measured by the same method as our alloys. Since it is the relative change in Curie temperature in which we are interested, these values give a good basis for determining this shift in Curie temperature.

There are several experimental indications which indicate that the magnetic effects in the 33 percent sample are at least as great as in the ANS sample. One of these is the lattice parameter versus temperature data in Figure 5 which shows a greater effect in the higher nickel alloys. This effect is known to peak at about 36 percent nickel. (Masumoto, 1931). Another is the Youngs modulus data of Guillaume (1920) which shows a broad maximum in the positive E versus T slope at compositions centered about 35 percent

nickel. The isotropic shear modulus appears to behave in a similar way. (Clark, 1962). Thus, it seems to be a reasonably conservative estimate to assume the same size magnetic effect for B and C' in the 31 and 33 percent samples as in the ANS sample. It is somewhat liberal to assume the same thing for the 29 percent sample. However, this sample plays a minor role. For the effect on the elastic constant C a more exact estimate of the composition effect can be made. This is due to the small size of the explicitly magnetic effect in its temperature dependence. The change in slope is seen to be much less than in B and C' and can nearly all be attributed to the change in slope in lattice parameter versus temperature. To do this we use

$$\frac{dC}{dT} = \frac{\partial C}{\partial T} + \frac{\partial C}{\partial v}\frac{\partial v}{\partial T} = \frac{\partial C}{\partial T} + \frac{\partial C}{\partial v} 3\left(\frac{1}{a}\frac{\partial a}{\partial T}\right) \qquad C\text{-}1$$

where v is the specific volume. If we make $\frac{\partial C}{\partial T} = 0$ then we can calculate $\frac{\partial C}{\partial v}$ from the linear portion of the curve above the Curie temperature and use this and measured values of $\Delta a/a$ versus temperature in

$$C = C_o + \frac{\partial C}{\partial v} 3 \frac{\Delta a}{a} \qquad C\text{-}2$$

to construct a C versus T curve. This nearly coincides with that measured by ANS. The assumption that $\frac{\partial C}{\partial T} = 0$ is justified on theoretical grounds (Huntington, 1958, p. 330). Moreover, using

$$\frac{dC}{dT} = \frac{\partial C}{\partial T} + \frac{\partial C}{\partial p}\,\frac{\partial p}{\partial v}\,\frac{\partial v}{\partial T} \qquad C\text{-}3$$

and the data given by Huntington (1958, pp. 274, 322, 324) to calculate $\frac{\partial C}{\partial T}$ we find that it is zero within experimental error for most of the materials for which adequate data are available.

Thus, it seems justifiable to use the procedure described above to calculate C versus T on the basis of the measured $\Delta a/a$ versus T of our alloys.

APPENDIX D: Model for Introducing Frequency Dependent Elastic Constants into the Debye-Waller Factor

To obtain a qualitative picture of how frequency dependent elastic constants would effect the Debye-Waller factor and through it the experimentally determined x-ray Debye temperature, we introduce a simple model for this frequency dependence. The qualitative picture should not be sensitive to the details of the model.

In Figure 12 is shown the frequency versus wave vector for our model. Up to some wave vector k there is a constant phase velocity, V_1, which is equal to the group velocity. At larger wave vectors there is a different phase velocity, V_2, which is equal to the group velocity in that range. The frequencies ω_1 and ω_2 defined by the figure are seen to be related by

$$\frac{\omega_1}{V_1} = \frac{\omega_2}{V_2} \qquad D-1$$

Using equation 3.21 from Section III we obtain this model

$$\eta = 4\pi N \left(\frac{a}{2\pi}\right)^3 \int_0^{\omega_m} \frac{\omega^2 d\omega}{V^2 U}$$

$$= 4\pi N \left(\frac{a}{2\pi}\right)^3 \left[\int_0^{\omega_1} \frac{\omega^2 d\omega}{V_1^3} + \int_0^{\omega_m} \frac{\omega^2 d\omega}{V_2^3} - \int_0^{\omega_2} \frac{\omega^2 d\omega}{V_2^3}\right] \qquad D-2$$

which gives

Figure 12

Dispersion Curve
for
Modified Debye Model

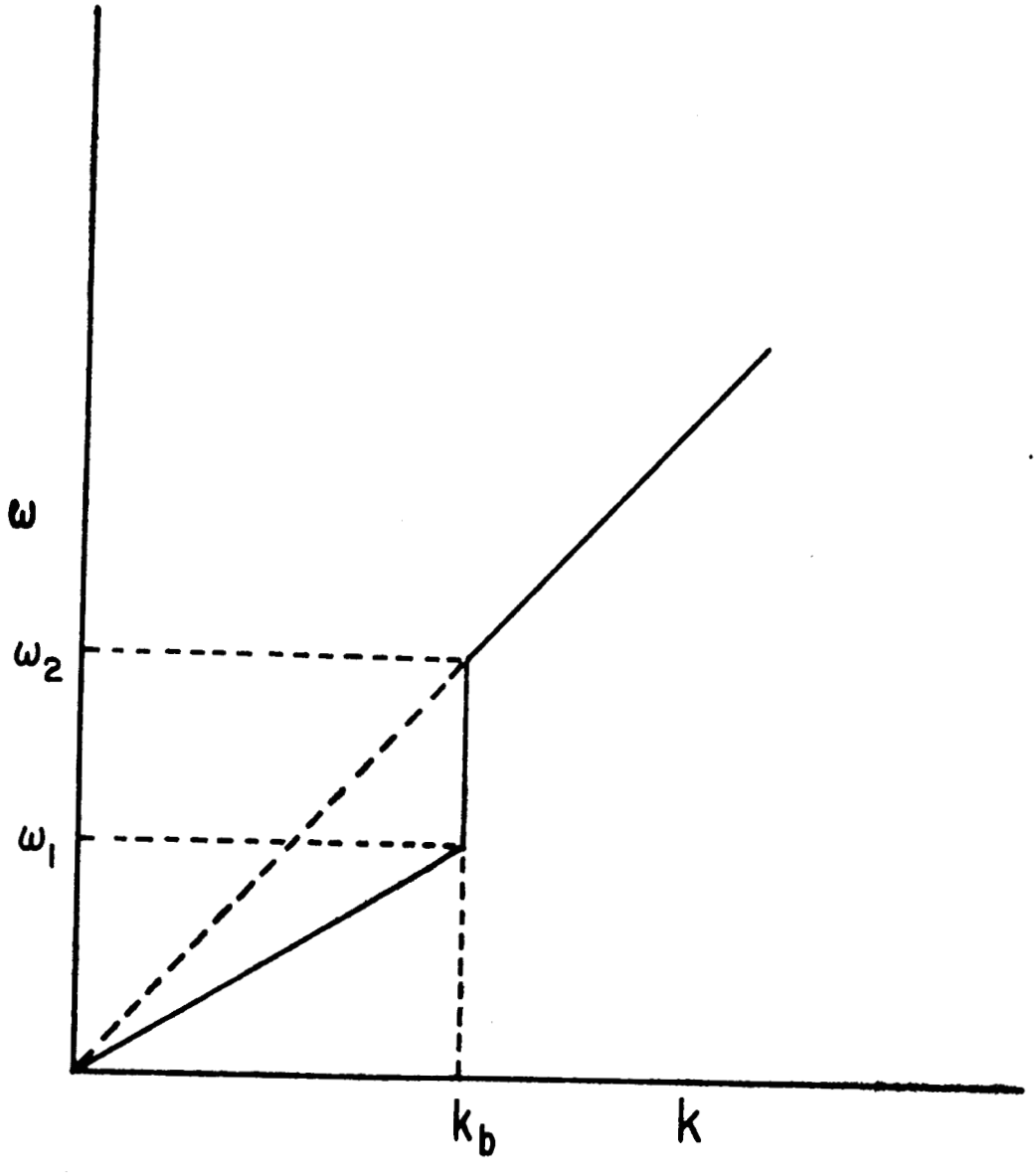
ω
ω2
ω1
kb
k

$$4\pi\left(\frac{a}{2\pi}\right)^3 \frac{N}{\eta} = 3\left(\frac{V_2}{\omega_m}\right)^3 \qquad D\text{-}3$$

Inserting this in equation 3.22 we have

$$2M = \frac{\hbar \kappa^2 S^2}{3m}\, 3\left(\frac{V_2}{\omega_m}\right)^3 \sum_j P_j \qquad D\text{-}4$$

where using procedures similar to Section III

$$P = \int_0^{\omega_m} \frac{(n+\frac{1}{2})\,\omega\, d\omega}{V^2 U} = \left(\frac{kT}{\hbar}\right)^2 \left[\int_0^{x_m} \frac{1}{V^2 U} \frac{x\,dx}{e^x - 1} + \frac{1}{2}\int_0^{x_m} \frac{x\,dx}{V^2 U}\right]$$

$$= \frac{\omega_1^2}{V_1^3}\left[\frac{\phi(x_1)}{x_1} + \frac{1}{4}\right] + \frac{\omega_m^2}{V_2^3}\left[\frac{\phi(x_m)}{x_m} + \frac{1}{4}\right] - \frac{\omega_2^2}{V_2^3}\left[\frac{\phi(x_2)}{x_2} + \frac{1}{4}\right] \qquad D\text{-}5$$

which gives

$$2M = \frac{\hbar}{m} \kappa^2 S^2 \sum_j \left\{ \frac{1}{\omega_m}\left[\frac{\phi(x_m)}{x_m} + \frac{1}{4}\right] + \right.$$

$$\left. + \frac{\omega_1^3}{\omega_m^3}\left(\frac{V_2}{V_1}\right)^3 \left[\frac{1}{\omega_1}\left(\frac{\phi(x_1)}{x_1} + \frac{1}{4}\right)\right] - \left(\frac{\omega_2}{\omega_m}\right)^3 \left[\frac{1}{\omega_2}\left(\frac{\phi(x_2)}{x_2} + \frac{1}{4}\right)\right] \right\}$$

$$= \frac{12\hbar^2}{mk}\frac{\sin^2\theta}{\lambda^2}\sum_j\left\{\frac{1}{\Theta_m}\left(\frac{\phi(x_m)}{x_m}+\frac{1}{4}\right)+\right.$$

$$\left.+f^3\left[\frac{1}{\Theta_1}\left(\frac{\phi(x_1)}{x_1}+\frac{1}{4}\right)-\frac{1}{\Theta_2}\left(\frac{\phi(x_2)}{x_2}+\frac{1}{4}\right)\right]\right\} \qquad D\text{-}6$$

following Section III. We have introduced a parameter f defined by

$$\Theta_2 = f\,\Theta_m \qquad \text{or} \qquad \omega_2 = f\,\omega_m$$

which is a measure of where the change in elastic constants occur relative to the cutoff frequency. The experimental Debye temperature in this model is then defined by

$$\frac{1}{\Theta_M}\left\{\frac{\phi(x_m)}{x_m}+\frac{1}{4}\right\} = \frac{1}{\Theta_m}\left(\frac{\phi(x_m)}{x_m}+\frac{1}{4}\right)+$$

$$+f^3\left[\frac{1}{\Theta_1}\left(\frac{\phi(x_1)}{x_1}+\frac{1}{4}\right)-\frac{1}{\Theta_2}\left(\frac{\phi(x_2)}{x_2}+\frac{1}{4}\right)\right] \qquad D\text{-}7$$

Applying this to the iron-nickel alloys we make $\Theta_1 = f\Theta_2$ where Θ_2 is the Debye temperature calculated from the elastic constants when the magnetic effects are included; then $\Theta_2 = f\Theta_4$ and $\Theta_m = \Theta_4$ where Θ_4 is the Debye temperature calculated from the elastic constants when the magnetic effects are absent. The value of Θ_M was then calculated by this method over the temperature range of interest for several values of f. The results are shown in Figure 13.

Figure 13

Debye Temperature Versus Temperature
for the Modified Debye Model
Applied to the 33 Percent Nickel Alloy

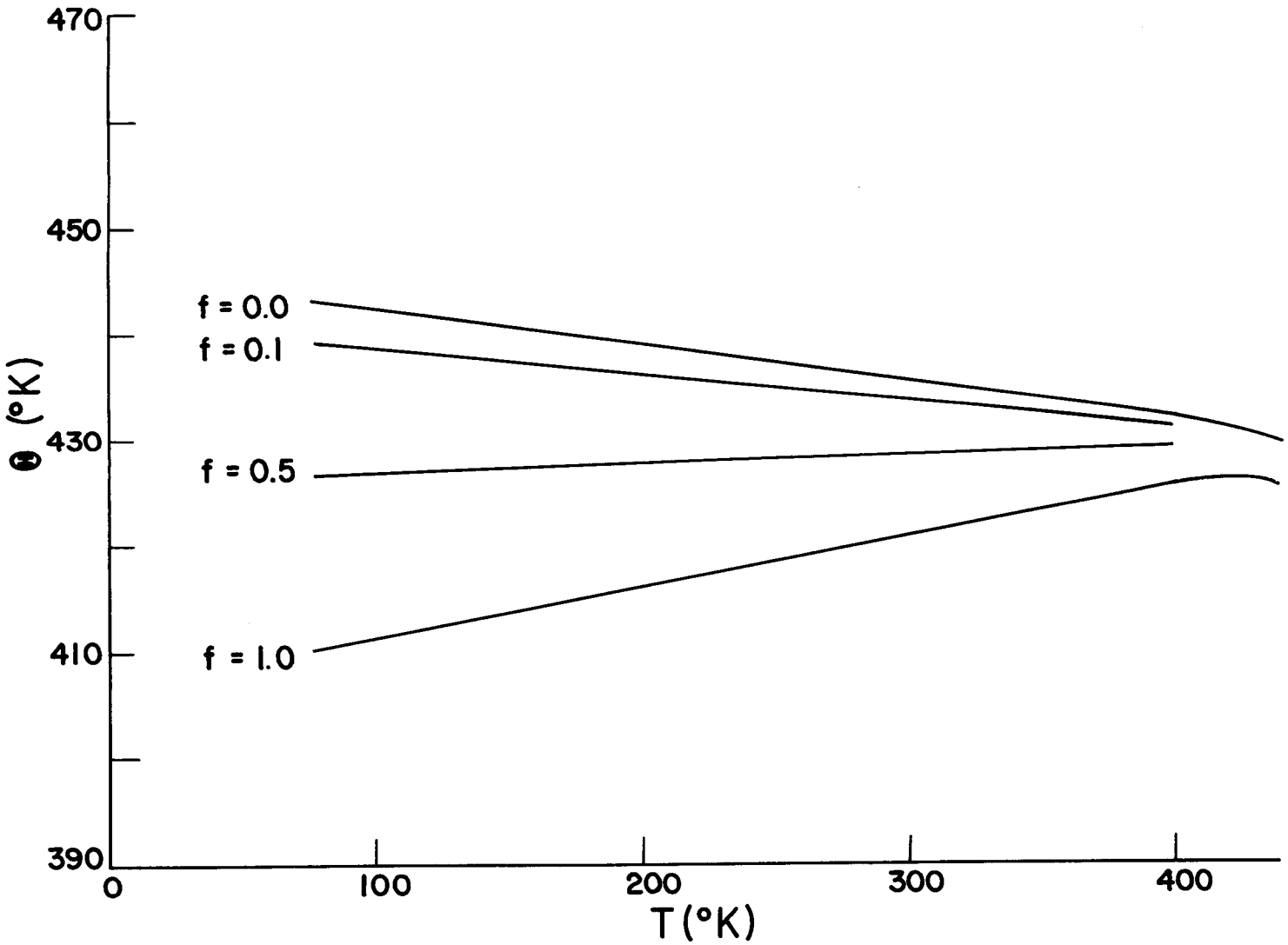
470
450
430
410
390
Θ (°K)
f = 0.0
f = 0.1
f = 0.5
f = 1.0
0
100
200
300
400
T (°K)

APPENDIX E: Alternate Form of the Döring Term

From the definition of the bulk modulus B we have for constant magnetization, I,

$$\frac{1}{B_I} = \left.\frac{\partial v}{\partial p}\right|_{\sigma} \qquad E\text{-}1$$

where v is specific volume, p is pressure and σ is magnetization per unit mass. At constant field, H,

$$\frac{1}{B_H} = \left.\frac{\partial v}{\partial p}\right|_{H} \qquad E\text{-}2$$

But we can write

$$\left.\frac{\partial v}{\partial p}\right|_{H} = \left.\frac{\partial v}{\partial p}\right|_{\sigma} + \left.\frac{\partial v}{\partial \sigma}\right|_{p} \left.\frac{\partial \sigma}{\partial p}\right|_{H} \qquad E\text{-}3$$

Combining equations E-1 through E-3, we get

$$\frac{1}{B_I} - \frac{1}{B_H} = -\left.\frac{\partial v}{\partial \sigma}\right|_{p} \left.\frac{\partial \sigma}{\partial p}\right|_{H} \qquad E\text{-}4$$

We can write

$$\frac{\partial v}{\partial T} = \left.\frac{\partial v}{\partial T}\right|_{\sigma=0} + \frac{\partial v}{\partial \sigma}\frac{\partial \sigma}{\partial T} \qquad E\text{-}5$$

Solving this for $\frac{\partial v}{\partial \sigma}$ and substituting into equation E-4, we get

$$\frac{1}{B_I} - \frac{1}{B_H} = - \frac{\left(\frac{\partial v}{\partial T} - \frac{\partial v}{\partial T}\Big|_{\sigma=0}\right) \frac{\partial \sigma}{\partial p}\Big|_H}{\frac{\partial \sigma}{\partial T}\Big|_p}$$

$$= - \frac{(3\alpha - 3\alpha_0) \frac{\partial \sigma}{\partial p}\Big|_H}{\frac{\partial \sigma}{\partial T}\Big|_p} \qquad E\text{-}6$$

where α is the coefficient of linear expansion of the ferromagnetic material and α_0 is the coefficient of linear expansion in the absence of ferromagnetism.

Using

$$\frac{\partial \sigma}{\partial p} = - \frac{1}{\rho} \frac{\partial v}{\partial H} \simeq -4\,(10)^{-9} \frac{emu}{dyne/cm^2} \qquad E\text{-}7$$

from ANS data. Also from their paper

$$\alpha - \alpha_0 = -1.2\ (10)^{-5} \frac{1}{C^\circ}$$

at room temperature. The value of α_0 used was their α observed above the Curie temperature. From the data of Kouvel and Wilson (1961), we estimate

$$\frac{\partial \sigma}{\partial T} = .3 \ \frac{emu}{C^\circ}$$

so

$$\frac{1}{B_I} - \frac{1}{B_N} = -.16\ (10)^{-12}\ \frac{cm^2}{dyne}$$

Using the data of ANS we get

$$\frac{1}{B_{extrapolated}} - \frac{1}{B_{observed}} = -\ .2\ (10)^{-12}\ \frac{cm^2}{dyne}$$

Thus, it is reasonable to attribute the magnetic effects in B to the Döring term.

APPENDIX F: Calculation of Debye Temperatures from Elastic Constants

In our notation the Debye temperature in the Debye approximation is given by

$$\Theta = \frac{h}{k}\left(\frac{3\nu}{4\pi}\right)^{1/3}\frac{1}{a}\,v_m \qquad F\text{-}1$$

which follows from equation 3.23. Here v_m is the isotropic average velocity of the vibrational waves. We let

$$v_m = \sqrt{\frac{\mu_m}{\rho}} \qquad F\text{-}2$$

where ρ is the density and μ_m is an average elastic constant given by

$$\frac{1}{\mu_m} = \frac{1}{3}\left[\frac{1}{B_H + \frac{4}{3}\mu_H} + \frac{2}{\mu_H}\right] \qquad F\text{-}3$$

for the x-ray Debye temperature. (The specific heat Debye temperature involves a different average over the longitudinal and transverse elastic constants.) Following Anderson (O. L. Anderson, 1963) we use

$$B_H = \frac{1}{2}\left(B_R + B_V\right) \qquad F\text{-}4$$

and

$$\mu_H = \frac{1}{2}\left(\mu_R + \mu_V\right) \qquad \text{F-5}$$

where the R and V subscripts refer to the Reuss and Voight isotropic averages of the elastic constants (Huntington, 1958, p. 317) given by

$$B_R = B_V = \frac{1}{3}\left(c_{11} + 2c_{12}\right) \qquad \text{F-6}$$

$$\mu_V = \frac{1}{5}\left(c_{11} - c_{12} + \frac{3}{4}c_{44}\right) = \frac{1}{5}\left(2C' + 3C\right) \qquad \text{F-7}$$

$$\mu_R = \frac{5}{4S_{11} - 4S_{12} + 3S_{44}} = \frac{5}{\frac{2}{C'} + \frac{3}{C}} \qquad \text{F-8}$$

for cubic crystals.

SECTION X

LITERATURE CITED

Alers, G. A., J. R. Neighbours and H. Sato (1960), J. Phys. Chem. Solids, 13, 40.

Anderson, O. L. (1963), J. Phys. Chem. Solids, 24, 909.

Anderson, P. W. (1963), Solid State Physics, Seitz and Turnbull, eds. (Academic Press, New York), Vol. 14, p. 99.

Bethe, H. (1933), Handbuch der Physik, (Springer-Verlag, Berlin), Vol. 24, Part 2, p. 595.

Blackman, M. (1955), Handbuch der Physik, S. Flugge, ed. (Springer-Verlag, Berlin), Vol. 7, Part 1, p. 325; (1956), Acta. Cryst., 9, 734.

Born, M. (1942a), Proc. Roy. Soc. A., 180, 397; (1942b), Proc. Phys. So., 54, 362; (1942c) Rep. Prog. Phys. (Physical Society), 9, 294.

Born, M. and T. v. Karman (1912), Physical Zeit. 13, 297; (1913), 14, 15.

Bozorth, R. M. (1950), Ferromagnetism, (D. Van Nostrand Co.)

Chevenard, M. P., Comptes Rendus 171, 93 (1920).

Chipman, D. R. (1960), J. Appl. Phys., 31, 2012.

Chipman, D. R. and A. Paskin (1959), J. Appl. Phys., 30, 1998.

Clark, C. A. (1962), Instn. Elec. Eng. Proc., 109 pt. B (Supp) n22, p. 389.

Debye, P. (1912), Ann. d. Physik, 39, 789; (1914), 43, 49.

de Launay, J. (1956), Solid State Physics, Seitz and Turnbull, eds. (Academic Press, New York), Vol. 6, p. 219.

De Wames, R. E., T. W. Wolfram and G. W. Lehman (1963), Phys. Rev., 131, 528.

Engler, O. (1938), Ann. Phys. Lpz., 31, 145.

Faxen, H. (1918), Ann. d. Physik, 54, 615.

Flinn, P. A., G. M. McManus, and J. A. Rayne (1961), Phys. Rev., 123, 809.

Freeman, A. J. and R. E. Watson (1961), Acta. Cryst., 14, 231.

Fuchs, K. (1936), Proc. Roy. Soc. (L), A153, 622.

Guillaume, C. E., Comptes Rendus, 171, 93 (1920).

Herbstein, F. H. (1961), Adv. in Phys., 10, 313.

Huntington, H. B. (1958), Solid State Physics, Seitz and Turnbull, eds. (Adademic Press, New York), Vol. 7, p. 213.

James, R. W. (1954), The Optical Principles of the Diffraction of X-Rays, (G. Bell and Sons Ltd., London).

Kagan, A. S. and Y. S. Umanskii (1962), Sov. Phys. Sol. St., 3, 1956.

Kondorsky, E. I. and V. L. Sedov (1960), J. Appl. Phys., 31, 331S.

Kouvel, J. S. and R. H. Wilson (1961), J. Appl. Phys., 32, 435.

Maradudin, A. A. and P. A. Flinn (1963), Phys. Rev., 129, 2529.

Maradudin, A. A., E. W. Montroll and G. H. Weiss (1963), Solid State Physics, Seitz and Turnbull, eds. (Academic Press, New York), Supplement 3.

Mason, W. P. (1953), Rev. Mod. Phys., 25, 136.

Masumoto, H. (1931), Sci. Rept., Tohoku Univ., 20, 101.

Nilsson, N. (1957), Arkiv Fysik, 12, 247.

Ott, H. (1935), Ann. d. Physik, 23, 169.

Owen, M. A. and E. L. Yates (1937), Proc. Phys. Soc. (L), 49, 178.

Paskin, A. (1957), Acta. Cryst. 10, 667; (1960), J. Appl. Phys., 31, 318S.

Simerska, M. (1962), Czech. J. Phys., 12, 858.

Waller, I. (1923), Zeit. f. Physik, 17, 398; (1928), 51, 213.

Young, R. A. (1961), Background Intensities in Single Crystal Diffractometry; Technical Report No. 2, Project No. A-389, Georgia Inst. of Tech., Atlanta, Ga.

Zener, C. and S. Bilinsky (1936), Phys. Rev., 50, 101.